Bachelor-Thesis in Physics

August 2018

Preparatory work for a lab course with a hybrid air shower detector

---

presented by
Hanja Wehrle

at the
Faculty of Mathematics, Computer Science and Natural Sciences
at the RWTH Aachen University

The present work was submitted to the
Physics Institute III A

Dr. rer. nat., Professor Thomas Bretz (1^{st} examiner)
Dr. rer. nat., Privatdozent Oliver Pooth (2^{nd} examiner)

Contents

1 Introduction

Stars, planets, galactic nebulae, pulsars and infinite expansions. The universe is a great mystery and scientists all over the planet are researching in hopes for revolutionary breakthroughs. 1912 Victor Hess measured the ionizing rate with electroscopes by bringing them up to an altitude of more than 5000 meters in a hot air balloon. He measured rising rates with rising altitudes, concluding that this phenomena can only be explained by high energetic radiation from out of space [1].

Starting with the work and determination of Victor Hess the world is on its way to answer mysterious questions about our universe. By analysing the particles arriving at Earth, reconstructing their energies and the arrival directions the source can be found and new information on the human existing and other phenomena can be learned. New measuring methods are thought of and exciting tools are improved on a regular basis.

For upcoming physicists it is of great importance to learn about new measuring methods and results but also to gain experience in dealing with measurement tools. This thesis gives students the opportunity to work with detectors, measuring cosmic rays and learning more about the measuring techniques. It is written to prepare a future lab course and give a roadmap to its implementation.

With this thesis a lab course for students, measuring with a hybrid air shower detector, can be realized. The hybrid detector consists of an array of scintillating detectors and the imaging air-Cherenkov telescope FAMOUS. Both detectors are presented in this work. Measurements and analysis' with each detector are shown. Additionally possible setups and triggering settings for the hybrid detector are depicted. As a proof of concept measurements with the hybrid air shower detector were recorded and the results analysed. For further work on the implementation of the lab course, possible

tasks for the students are explained and possible adjustments on the measuring systems, which should be executed before the lab course is realized, are mentioned in this work.

2

Cosmic rays

This thesis describes the detection of cosmic rays with a hybrid air shower detector based on silicon photomultipliers (SiPMs). To give an understanding of the principles for this work, the relevant physical matters are discussed in the following.

Particles reaching Earth from outer space with high energies are called cosmic rays. They were first discovered by Victor Hess in 1912 and consist to 98% out of nuclei and 2% are made up by electrons. The nuclei are divided into 87% protons, 12% $\alpha-$particles and 1% heavier nuclei. Most of the particles come from stellar productions or supernovae. The particle energies have a range from a few MeV up to a few EeV. The rate of cosmic rays arriving at the Earth decreases with rising energies shown in Figure 2.1. The difference in flux and energy leads to mainly two types of measurements for cosmic rays [2, 3].

2.1 Primary and secondary particles

Primary cosmic rays with high fluxes and low energies do not have enough energy to be detected at surface level. Due to the high rate a small detector area is enough to detect the particles directly with detectors in the atmosphere such as the Fermi Gamma-ray Space Telescope [5]. Primary cosmic rays can be measured directly for particle energies of up to 100 TeV [3].

For primary particles with lower fluxes, a larger area of detectors is needed, which is not realizable in space. These particles have enough energy (more than several TeV) to interact with the particles in the atmosphere and to trigger an air shower which will reach the surface. These air showers have a large expansion and can be measured with

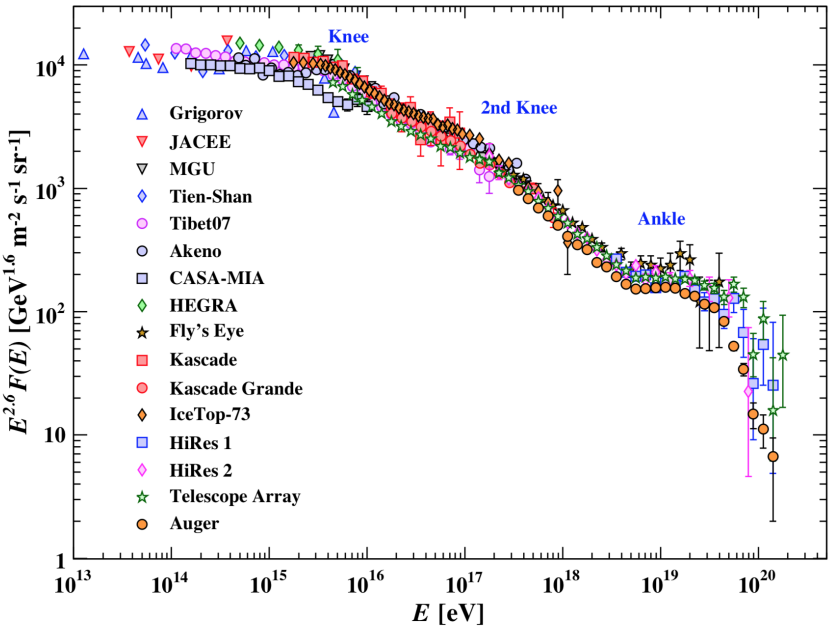

Figure 2.1: Dependency between the flux and the energie of cosmic rays [4].

detector arrays covering a large area on the surface e.g. the Pierre Auger Observatory in Argentina [6].

An air shower occures when a high energetic particle interacts with the particles in the atmosphere and creates new secondary particles which create other particles building so called cascades as shown in Figure 2.2. There is a difference between different cascades depending on the particle that induces them. Proton-nuclei-interaction mainly takes place in hadronic cascades. These interactions mainly produce pions (π) which decay into muons (μ) and photons (γ) as well as other particles [3]. In electromagnetic cascades electrons and positrons interact via pair production and create photons which generate electrons and positrons due to bremsstrahlung. The muonic component of a shower is made up out of muons, which decay into electrons or positrons but mostly reach the surface due to their relativistic speeds and time dilation. Muons are the most noumerous charged particles at the surface.[3, 4]

Some of the most common decays in air showers are shown below. Equation 2.1 describes decays in hardronic cascades and equation 2.2 in electromagnetic cascades [3].

$$\begin{aligned} \pi^0 &\rightarrow 2\gamma \\ \pi^+ &\rightarrow \mu^+ + \nu_\mu \\ \pi^- &\rightarrow \mu^- + \overline{\nu_\mu} \end{aligned} \tag{2.1}$$

$$e^+ + e^- \rightarrow 2\gamma \tag{2.2}$$

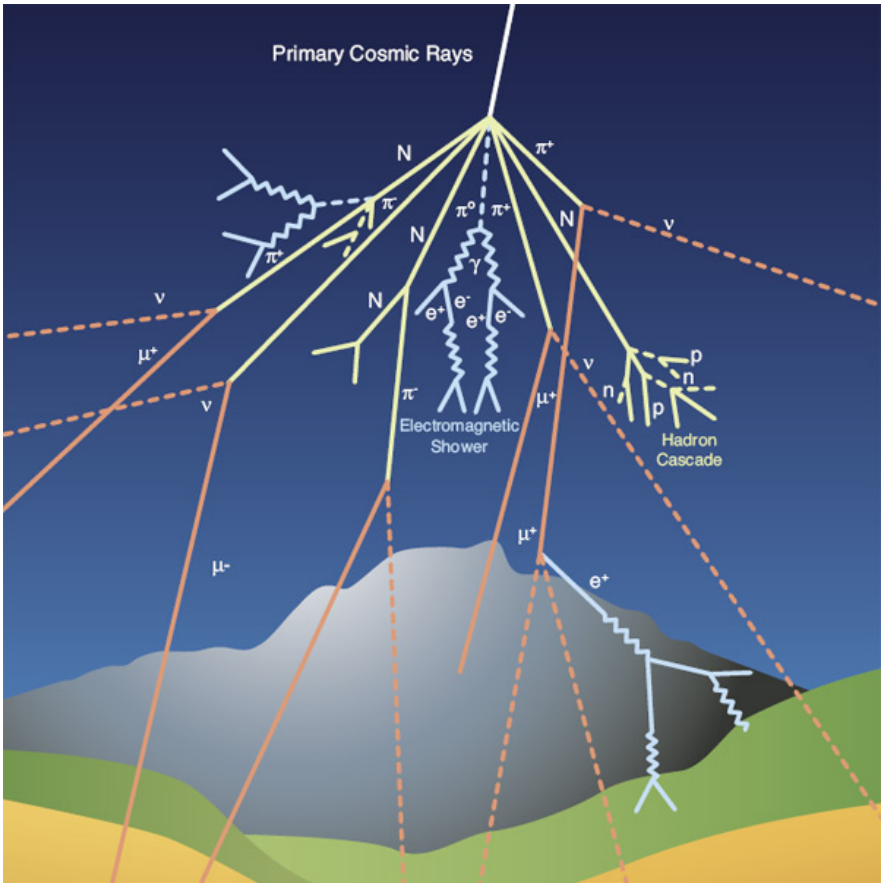

Figure 2.2: Schematic of cosmic rays and shower cascades [7].

Two of the main detection techniques from the ground are the air-Cherenkov technique and the particle observation in large areas [3].

2.2 Air-Cherenkov technique

If a particle in a medium with a refractive index n reaches a speed of $v_c > \frac{c_0}{n}$ Cherenkov light is emitted under an angle of $\sin(\vartheta_c) = \frac{c_0}{nv}$.

This effect appearers in the atmosphere as well, where the refractive index is dependent on the height h. At standard atmospheric pressure at sea level the refractive index equals 1.00029. For Cherenkov light produced in the atmosphere by a shower it is expected that the Cherenkov beam is within 6° of the shower axis. [2, 3]

The beams of Cherenkov light can be measured from the surface with an imaging air-Cherenkov telescope (IACT).

2.3 Particle detection with large arrays

For air showers induced by high energetic primary particles (> 50 TeV), a large a number of secondary particles reach the surface [3]. These particles can be detected with surface detectors (refered to as air shower arrays), where air showers have a wide spread, so a detector array with a large surface coverage is needed. Examples for these detector arrays are the High-Altitude Water Cherenkov Observatory (HAWC) in Mexico [8] or the Pierre Auger Observatory in Argentina [6]. Both arrays work with large water tanks with photo-sensors and use Cherenkov light from particles crossing water tanks.

With large area observatories, it is possible to determinate the shower direction as well as estimating the energy of the primary particle. An estimation on the number of electrons and muons within the shower can be made as well [3].

2.4 Silicon photomultiplier

A silicon photomultiplier (SiPM) is a photo-sensor which can be used in IACTs or other detectors based on light detection e.g. in the First G-APD Cherenkov Telescope (FACT) or the First Auger Multi-pixel-photon-counter-camera for the Observation of Ultra-high-energy-cosmic-ray air Showers (FAMOUS). SiPMs are made of an array of Geiger-mode avalanche photo-diodes (G-APD)[9, 10].

A photo-diode is made up of a silicon p-n junction which creates a depletion region, free of charged particles. As soon as a photon is absorbed within the depletion region, it will create an electron-hole pair. A SiPM has a bias voltage which creates an electric field across the depletion region whereby the hole and electron will be accelerated by the anode or cathode. If the electron and hole have enough energy they will create more holes and electrons which results in the avalanche effect where every free particle results in more holes and electrons until the energy per particle is to low. This results in a voltage detection when a photon is absorbed [11].

2.5 Scintillators

Entering a medium, a particle loses energy per distance within the medium ($\frac{dE}{dx}$). In a scintillator the energy loss is due to atomic excitation within the material. After a short period of time the energy is set free by light emission (UV- or visible light mostly, dependent on the material). In general, it is distinguished between inorganic and organic scintillators [12].

Inorganic scintillators have a crystalline structure, create up to 40000 photons per MeV and have decay times in the order of microseconds. The materials are rather expensive and are mainly used in X-ray and gamma spectroscopy and medical imaging [12].

Organic scintillators, on the other hand, are mostly plastics or liquid solutions. They produce up to 10000 photons per MeV, have decay times within nanoseconds and they are relatively inexpensive. Organic scintillator find more applications in triggering and places a quick response is necessary.

3

Air shower array

On the roof of the Physikzentrum of the RWTH Aachen University, an air shower array is installed, shown in the Figure 3.1. It consists of an arrangement of six detectors based on liquid scintillators and SiPMs.

Figure 3.1: Picture of the setup on the roof of the Physikzentrum with the air shower array. Detector 6 can be seen in the front, photographed from west.

The setup has been constructed for a laboratory course on astroparticle physics for the particle physics or astroparticle physics and cosmology master students. In the lab experiment the students have to measure and reconstruct cosmic air showers.[1]

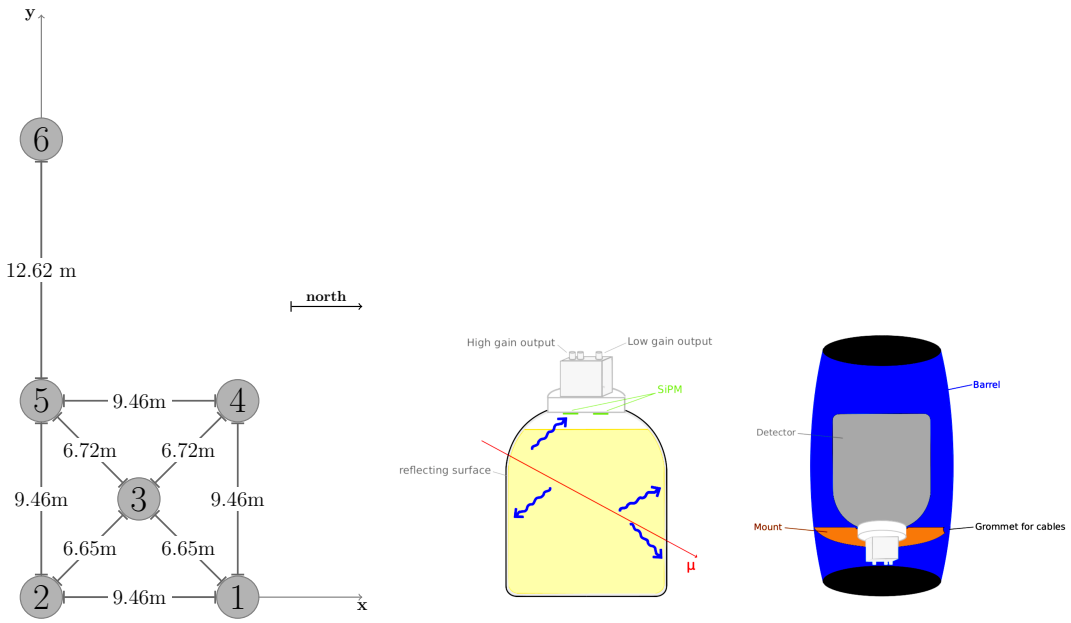

(a) Arrangement. **(b)** Cross section of one detector [14].

Figure 3.2: The air shower array and the detector barrels. a) Arrangement of the detectors on the roof of the Physikzentrum. b) Cross section of one detector in a barrel with the visualisation of the processes when a particle passes.

3.1 Setup and DAQ system of the air shower array

The organic scintillators for the particle detection are placed in containers, covered with reflecting color. On the bottom a silicon photomultiplier (SiPM) is installed registering light signals and sending two signals at detection, one to a triggering system and one for the data recording. The detectors are protected by rain barrels covered with reflecting material. These barrels protect the containers from environmental influences as well as it makes sure surroundings are saved in case of any leaks. The reflecting material is to minimize the influence of the heat during daytimes on measurements. The detectors' positions on the roof are shown in Figure 3.2a while Figure 3.2b displays a schematic representation of the construction of a detector.

The SiPMs send two signals, one negative and one positive. The former is directed into a Nuclear Instrumentation Module standard (NIM) triggering system. The triggering system corresponding mechanisms are explained in Figure 3.3. The system triggers for signals above an adjustable threshold and only if two detectors pass the threshold

[1] There are a more detailed describtions on the lab course in [13, 14]

within a ≈ 80 ns window[2]. As soon as the triggering signal reaches a DRS 4 board, it saves signals for one microsecond. For each entering signal 1024 samples in time and voltage are saved. The entering signals consist of the six positive SiPM signals, both boards are connected to three of those signals. They are not triggered simultaneously since the signal reaches one board first and is lead to the second board afterwards. To correct the delay the inverted triggering signal is recorded on both boards as well.

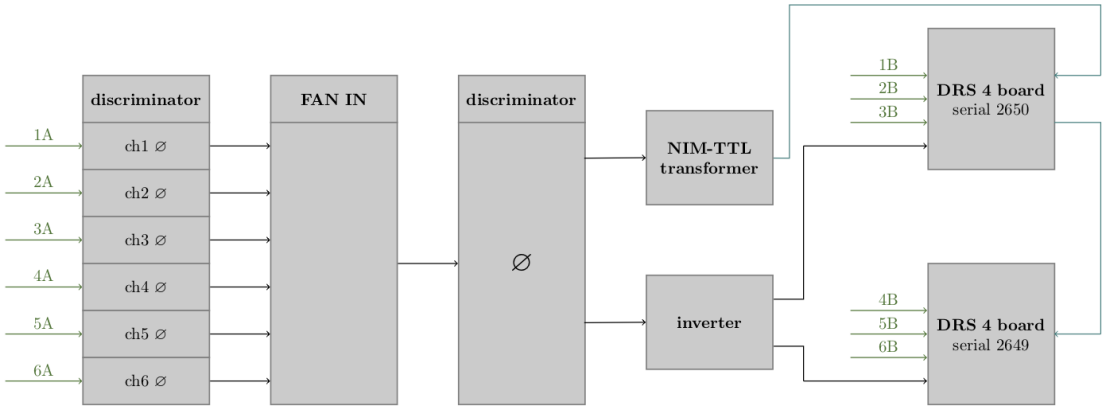

Figure 3.3: Schematic visualisation of the air shower array triggering system. The signals pass a discriminator are summed and pass the discriminator again. Afterwards the summed signal is passing to the DRS 4 boards for triggering. The signals entering the triggering system (A1 to A6) are the negative signals from the SiPM and the signals (B1 to B6) are the positive SiPM signals which are recorded by the DRS4 boards. Adapted from [14].

The data acquisition is shown in Figure 3.3. The discriminator returns a 800 mV and ≈80 ns wide squarewave signal if the signal is higher than the adjusted threshold. The FAN IN module adds all entering signals and multiplies them with $\frac{1}{8}$. The threshold for the totalized signal is set in order to only trigger signals with at least two simultaneous hits. For the triggering mechanism the signal is turned into a TTL signal and for flagging the triggering signal the pulses are inverted and led to both boards. Except for the triggering signal after the inverter all signals have the same delay. There is no delay due to cables except for the last triggering part, since all wires are chosen with the same length and delay.

3.2 Event analysis and reconstruction

To characterize the air showers detected by the array one can analyse the event properties. This includes the reconstruction of events and the comparison between properties of all events. However, before further analysis, the data has to be calibrated by correcting the baseline and the electrical time delay between the two boards.

[2]If the hits are apart more than the squarewave signal, which the discriminator returns, is wide, the FAN IN will not pass the second discriminator. It is the longest time between two pulses which would still be recorded as a coincidence between two detectors.

The data taking process for the used dataset started on June 8^{th}. The measurement lasted for 216 hours till June 17^{th}. The trigger settings are listed in Table 3.1. The threshold settings do not change for all following measurements. During this measurement the array detected 18683 events which equals 1.44 events per minute.

Detector	1	2	3	4	5	6	Σ
Threshold [mV]	32	32.5	32.2	31.9	33	32.2	115

Table 3.1: Threshold settings for the measurement from June 8^{th} with 18683 detected events. The thresholds are set manually at the discriminator. Σ is the signal which the FAN IN module returns.

The recording program creates ROOT TTrees with the SiPM signal in millivolts, the event-time in nanoseconds as well as the timestamps for each event as UTC system-time and as passed time since starting the measurement.

In Figure 3.4, the uncorrected and corrected raw data are shown for one exemplifying event. The signals have a baseline at ≈ -200 mV and the two boards have a delay due to the triggering by a few nanoseconds. For the further breakdown the baseline and delay are corrected.

The baseline is corrected by adding the median of the first 200 samples. The median is used to level out irregular spikes due to the DRS 4 boards[3]. As seen in Figures A.1 and A.2, in the appendix, a correction with the mean is not as effective to set a zero-baseline.

While taking a look at the trigger signals on both boards one can see that they are shifted by a few nanoseconds. As seen in the triggering system (Fig. 3.3) all delays are the same. The time difference appears after the NIM to TTL transformation where the boards are triggered successively. The precise time difference ΔT fluctuates for every event around 12 ns to 16 ns, so the correction has to be done individually. The signals are synchronised by shifting every time trace by ΔT.

3.2.1 Data and statistics

In 9 days (777802 seconds) of measurement, 18683 events were detected. Some of those events can appear as random coincidences, e.g. the detectors where not triggered exclusivly by particles of one shower or backgrond noise passes the thresholds and triggers a coincidence. Nevertheless, at least two detectors have to be hit simultaneously and each hit has to pass a discriminator, the rate is expected to be low. With the single detector rates from [13, 14] one can calculate the rate for random coincidences R_{random} with two detectors.

For a single detector with a set threshold of 30 mV the rate is $R_{detector} = 10$ Hz [13, 14] and for a hit in coincidence, both signals have to enter the triggering module within $\tau = 80$ ns. τ can be set manually at the discriminating module. The hits per detector

[3]The spikes are not corrected, since the influence on the analysis and correction is to small to justify the amount of work.

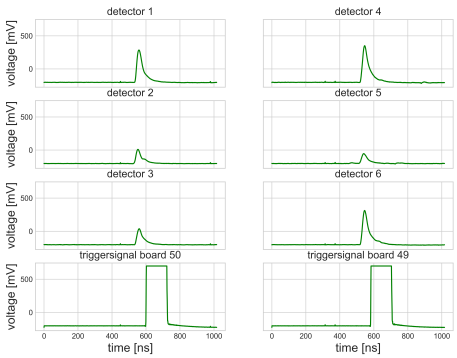

(a) Raw data

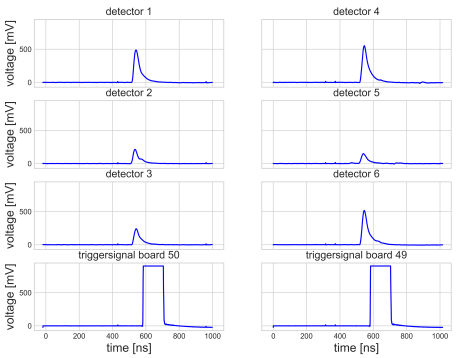

(b) Corrected data

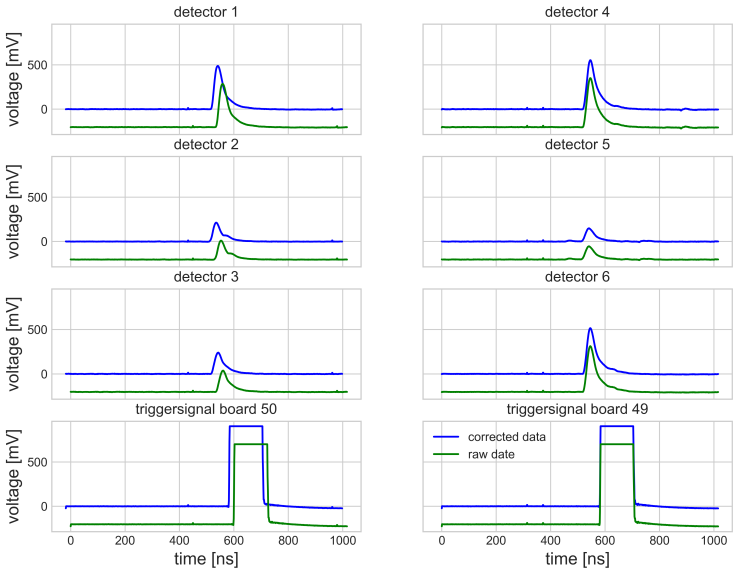

(c) Visualization of the data correction

Figure 3.4: 174^{th} event with 6 detector hits in coincidence. The raw data is corrected by shifting the baseline by the median of the first 200 voltage samples and by moving the times of one board by the time difference ΔT of the two triggering signals.

in Figure 3.5 are approximately the same for every detector, except detector 3, which has a higher rate than the others. This is expected since it is placed in the middle of the array with equal distances to detectors 1, 2, 4 and 5 which results in a higher chance to be hit in coincidence.

$$\begin{aligned} R_{random} &= 2 \cdot \tau \cdot R_{detector\,A} \cdot R_{detector\,B} \\ \implies R_{random} &= 1.6 \cdot 10^{-5}\ \text{Hz} = \frac{12}{9\ \text{days}} \end{aligned} \tag{3.1}$$

In equation 3.1, τ is the longest time between two pulses which would still be triggered as a coincidence. In this case it is the width of the squarewave signal from the discriminator. $R_{detectorA}$ and $R_{detectorB}$ are the single rates measured by the detectors A and B [15]. During this experiment the single rates are roughly the same for every detector.

As shown in equation 3.1, the rate R_{random} is low, as they are insignificant compared to the amount of detected events. There are other possibilities for random coincidences, e.g. two detectors triggered in coincidence measured randomly at the same time as two other detectors triggered in coincidence but for all other cases of random coincidences the individual rates are lower than $R_{detector} = 10$ Hz used in this calculation which makes the rate for random coincidences even lower.

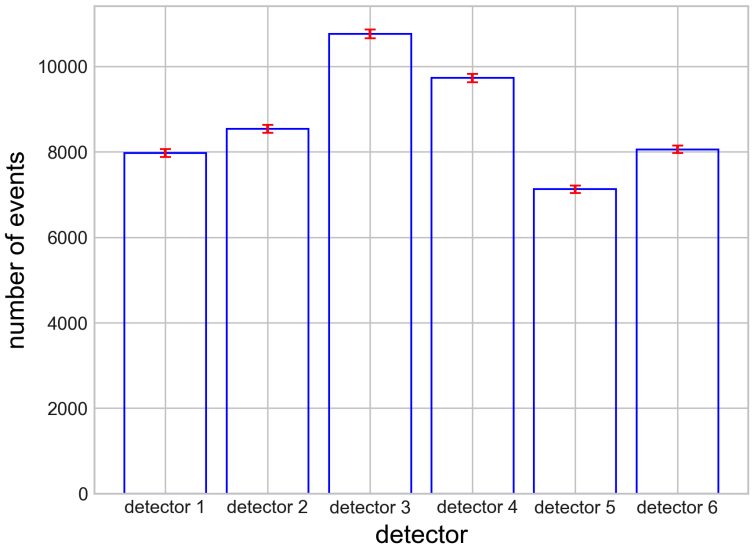

Figure 3.5: Hits per detector. The seen errors are assumed to be errors from the Poisson distribution as $\sigma = \sqrt{N}$, where N is the number of hits.

The event multiplicity (shown in Figure 3.6) clearly evidences that most of the showers only hit two detectors. This is as expected since most showers will not hit inside the small array area or are not energetic enough.

For events which hit all six detectors it is expected that the average pulse height is higher compared to events which only hit two detectors. Although statistical high energy events can arrive in the array area and only hit fewer detectors.

Figures 3.7 and 3.8 take a closer look into the events and their multiplicity. In Figure 3.7 it can be seen that the maximal pulse height of each hit detector during an event sorted by the event multiplicity. As suspected the pulse height increases with the number of hit detectors.

As explained, while taking a look at the hits per detector (Figure 3.5), detector 3 lays in the middle of the array so it has the best opportunities to take part in a coincidence. This is affirmed in Figure 3.8 where detector 3 has the most hits in coincidence with detector 4. Further on one can see that detectors standing closer to each other are hit

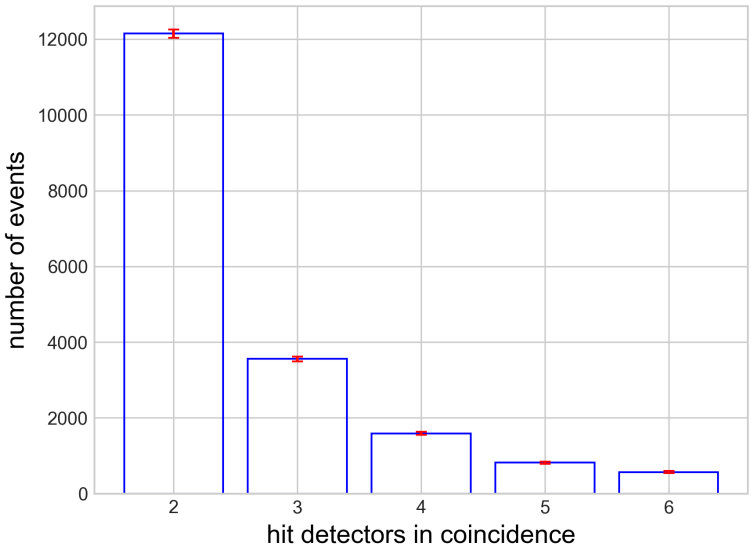

Figure 3.6: Event multiplicity for a multiplicity of events with 2, 3, 4, 5 and 6 hit detectors. The errors are assumed to be uncertainties from the Poisson distribution as $\sqrt{N}$, were N is the number of hits.

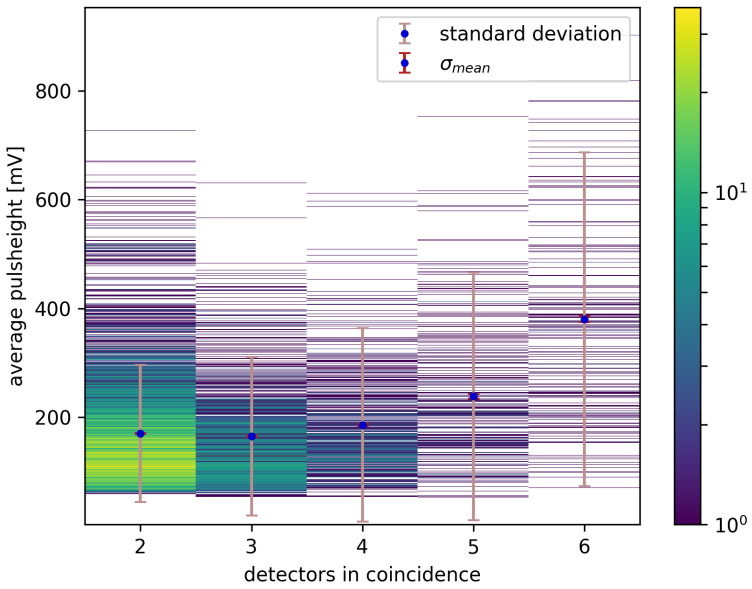

Figure 3.7: Maximal signal height in mV for each multiplicity. Every event was sorted by their multiplicity, for each hit detector the maximal signal height was registered and depicted in a two dimensional histogram. The colors correspond with the number of hits which have the shown pulse heights and appeared in events with the respective multiplicity.

more often. This is due to the fact that if a shower hits the array, the particle density is higher in the central part of the shower so it is more likely to hit a detector in this

area. Since this part of the shower is rather small, it will hit two detectors close to each other more probable than two detectors further apart.

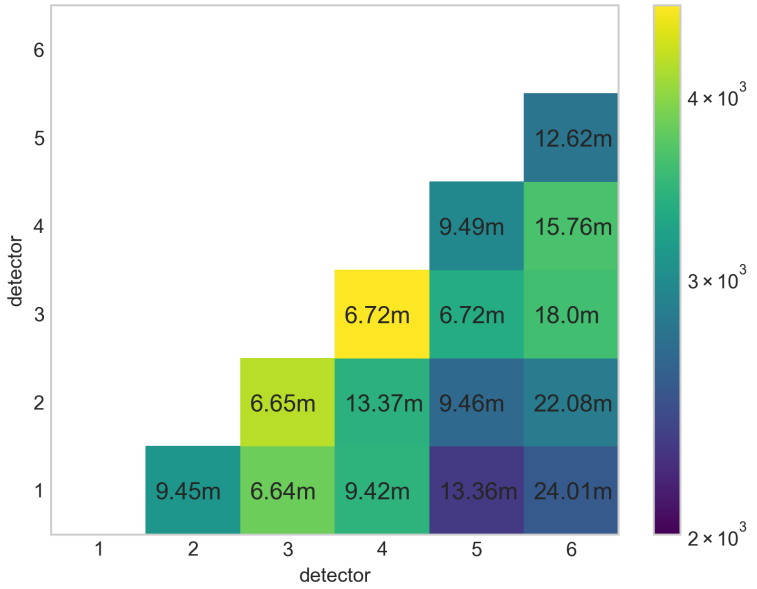

Figure 3.8: Histogram of the multiplicity of all hit combinations and distances between the detectors for all events. For the distances the error is $\sigma_{distance} = \frac{0.1}{\sqrt{12}}$ m. The colorscale describes the number of events which hit the shown combination of detectors.

3.2.2 Shower reconstruction

The approach for the shower reconstruction is based on [14]. During this work, the setup and tasks for the lab course were designed.

Mathematical approach

The shower direction can be reconstructed with a plane wave fit. A plane wave fit is appropriate, since the shower is so large that the small area of the air shower array does not perceive the curvature which the shower front has in reality. For this approach the influence of the azimuth angle and zenith angle on the shower arrival time at detectors in two dimensions can be seen in Figure 3.9. This means, the arrival direction of the shower can be calculated with the time difference of shower arrivals at the different detectors. The angles corresponding with the shower direction depend on the time difference between detector hits, on the speed of the shower front as well as on the distance between the detectors.

The velocity of particles within the shower can be approximated as the speed of light c. As seen in Figure 3.11 the distance between the shower front and the detector is

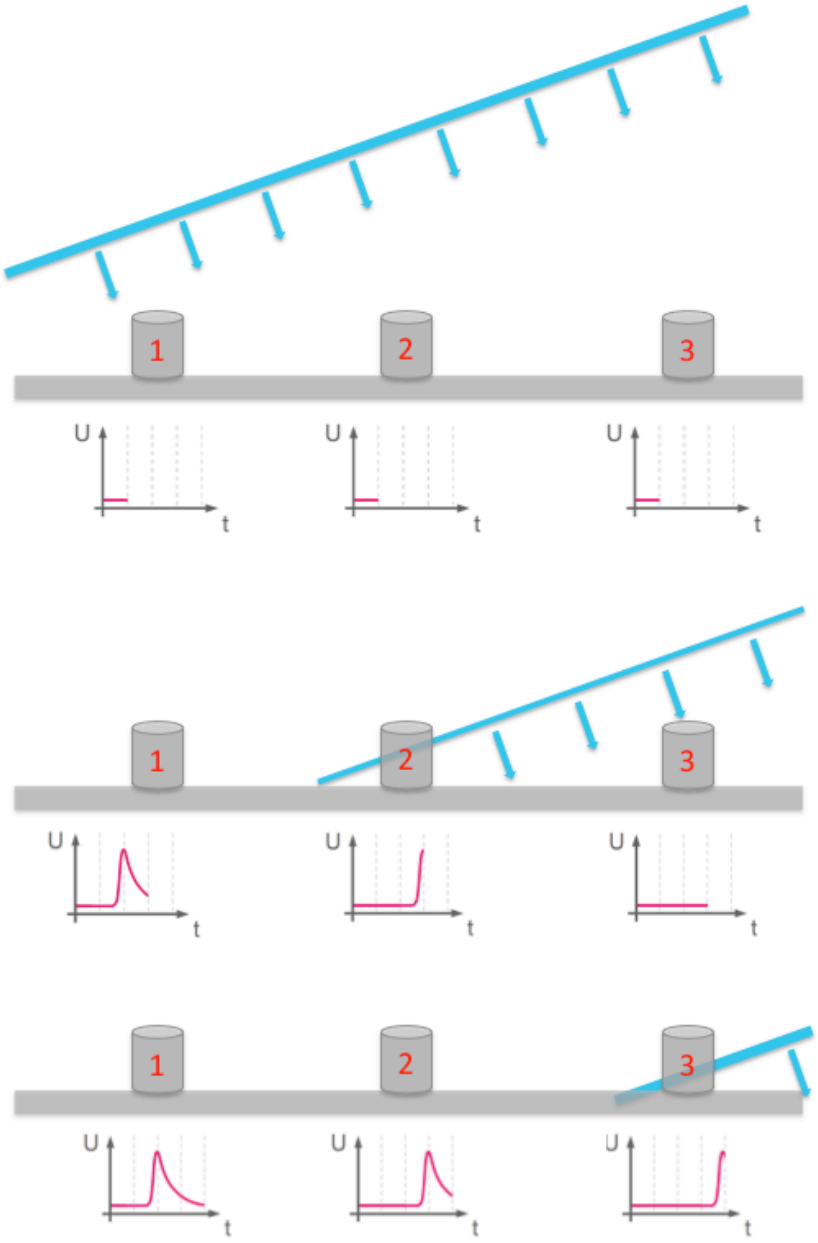

Figure 3.9: Two dimensional view on the distance of the shower front to the different detectors. Below the detectors the incoming signals are shown [13].

equal to the radius around detector i with $r_i = c \cdot \Delta t = c \cdot (t_0 - t_i)$. As a plane wave is presumed the shower front can be calculated by the tangential plane to the circles.

To calculate the shower direction, one can compute the surface normal to the front in Cartesian coordinates and transform it into spherical coordinates to get the azimuth angle and zenith angle (eq. 3.2). The calculations will be in two dimensions since all detectors are all in one level ($z = 0$). The azimuthal angle ϕ is pointing in the direction

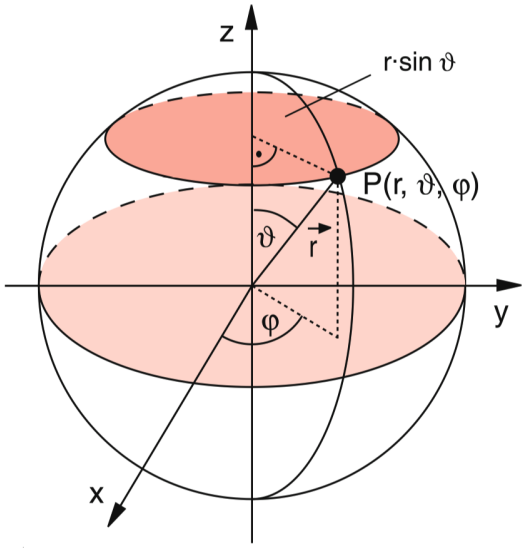

Figure 3.10: Visualisation of the angles θ and ϕ in spherical coordinates [16].

the shower is going to in the x-y-plane and the zenith angle θ is the angle to the z-axis from with direction the shower came. The orientation of the angles is shown in Figure 3.10.

$$\begin{aligned} \theta &= \arcsin \sqrt{n_x^2 + n_y^2} \\ \phi &= \arctan 2(n_y, n_x) \end{aligned} \tag{3.2}$$

In equation 3.2 n_x and n_y are defined by: $\overrightarrow{n} = n_x \overrightarrow{x} + n_y \overrightarrow{y} + n_z \overrightarrow{z}$. The formulas are the NumPy package in python.

In the following computations, d_i is the distance between the shower and detector i; r_i is the real distance and the circle radius. t_1, p_1(detector position) and d_1 will be the first detector to be hit by the air shower, for easier calculations this will be the origin of coordinates and starting point for the time measurement. The detector position is defined as $\overrightarrow{p_i} = x_i \cdot \overrightarrow{x} + y_i \cdot \overrightarrow{y} + z_i \cdot \overrightarrow{z}$, where at $z_i = 0$ since all detectors are standing on the same height.

For three hit detectors, not standing in one line, the analytical solution has the following ansatz:

$$\begin{aligned} d_2 &= \overrightarrow{p_2'} \cdot \overrightarrow{n} - t_2' \cdot c = 0 \\ d_3 &= \overrightarrow{p_3'} \cdot \overrightarrow{n} - t_3' \cdot c = 0 \end{aligned} \tag{3.3}$$

Whereat:

$$\begin{aligned} \overrightarrow{p_i'} &= \overrightarrow{P_1 P_i} = \overrightarrow{p_i} - \overrightarrow{p_1} \\ t_i' &= t_i - t_1 \end{aligned} \tag{3.4}$$

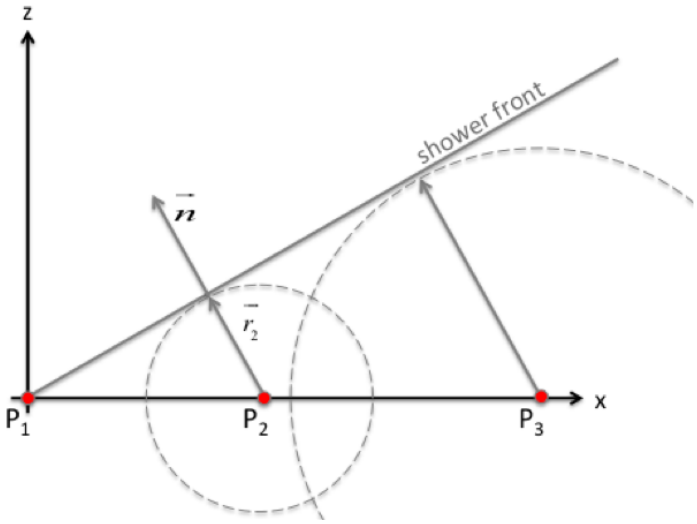

Figure 3.11: Illustration of the detector shower distance described by circles around the hit detectors. The shower front is moving with the speed of light so $r_i = c \cdot t_i$ [13].

$$\begin{aligned}
\overrightarrow{p_2'} \cdot \overrightarrow{n} - t_2' \cdot c = 0 \qquad &\wedge \qquad \overrightarrow{p_3'} \cdot \overrightarrow{n} - t_3' \cdot c = 0 \\
n_x + \frac{y_2' n_y - t_2' \cdot c}{x_2'} = 0 \qquad &\wedge \qquad n_x + \frac{y_3' n_y - t_3' \cdot c}{x_3'} \\
\implies n_y \Big(\frac{y_2'}{x_2'} - \frac{y_3'}{x_3'} \Big) + \frac{t_2' c}{x_2'} - \frac{t_3' c}{x_3'} = 0 &
\end{aligned}$$

$$\begin{aligned}
\iff n_y &= \frac{x_2' t_3' - x_3' t_2'}{x_3' y_2' - x_2' y_3'} \cdot c \\
\implies n_x &= -\frac{y_2' n_y + t_2' c}{x_2'}
\end{aligned} \tag{3.5}$$

With equations 3.2 and 3.5 the shower direction can be determinated (eq. 3.6). Adaptations were made for $x_2' = 0$ or $x_3' = 0$. To get a more precise result the angles θ and ϕ are caculated for every three detectors within the shower and for the final step the mean is used to get the azimuthal and zenith angles. The uncertainty on the angles is 2.9° estimated based on [13] and private communication with the author. This error results in the uncertainties appearing during the distance measurements and uncertainties on the arrival times. For the arrivals times the major uncertainty is due to the fact the particle path within the scintillator is unknown and the light could be created anywhere with in the detector material. The error is calculated with the area measurements of the scintillating material and the time light needs to travel the average distance. The uncertainty does not include the fluctuation within the shower, which effects the array since this can cause higher fluctuations within the arrival times and respectively results in a less precise reconstruction.

$$\begin{aligned}\theta &= \arcsin(\sqrt{n_y^2 + n_x^2}) = \arcsin\left(\sqrt{(\frac{x_2' t_3' - x_3' t_2'}{x_3' y_2' - x_2' y_3'} \cdot c)^2 + (-\frac{y_2' n_y + t_2' c}{x_2'})^2}\right) \\ \phi &= \arctan 2(n_y, n_x) + \pi = \arctan 2\big((\frac{x_2' t_3' - x_3' t_2'}{x_3' y_2' - x_2' y_3'} \cdot c), (-\frac{y_2' n_y + t_2' c}{x_2'})\big) + \pi\end{aligned} \tag{3.6}$$

In equation 3.6, π has to be aggregated to the azimuthal angle ϕ due to the chosen coordinate system for the shower arrangement.

For these computations at least three detectors have to be hit by the shower and they are not allowed to stand in one row, otherwise the considered coordinate system would be a 1D line where calculating two separate angles is not possible. If $x_i' = 0$ the calculations have to be adapted and it follows for $x_2' = 0$ ($x_3' = 0$ analogue):

$$\begin{aligned}n_y &= \frac{-t_2'}{y_2'} \cdot c \\ n_x &= -\frac{y_3' n_y + t_3' c}{x_3'}\end{aligned} \tag{3.7}$$

Results of the reconstruction

In Figure 3.12 the reconstructed shower direction, as well as the signal height in each detector and the time difference between t_1, the shower hitting the first detector (the shower hitting the first detector, here detector 2) and t_i, the shower hitting the regarded detector i are shown. As seen by looking at the times, the shower first hits detectors standing on the side the shower is coming from. In Figure 3.13 further events with reconstructed showers are seen.

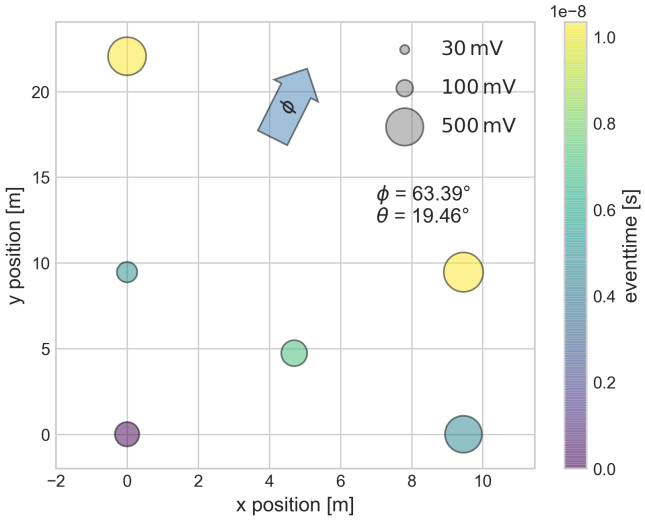

Figure 3.12: Shower reconstruction of event 174, seen in Figure 3.4. The color scale represents the arrival time in seconds of the shower at each detector, whereat t_1 is the start time as in previous deliberations. The diameter of the detectors in this plot is dependent on the maximal signal height in millivolts that the SiPM send out.

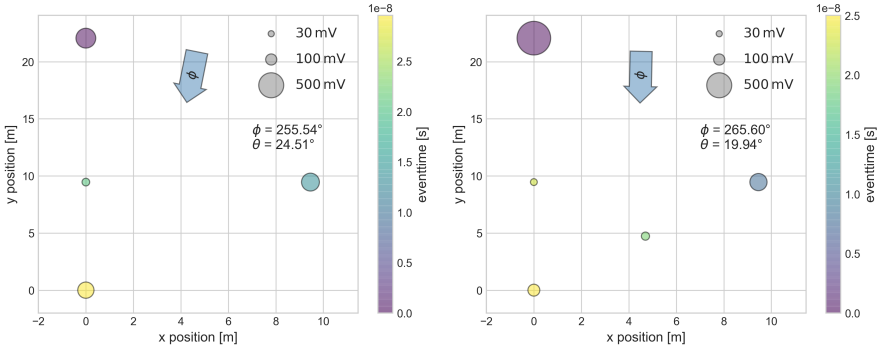

(a) Event 4

(b) Event 16

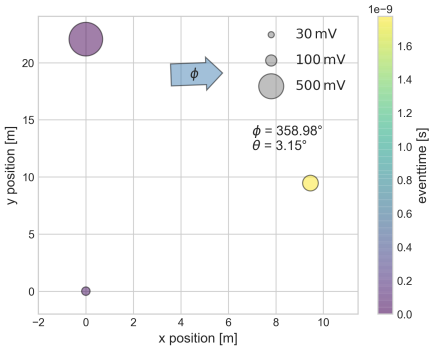

(c) Event 24

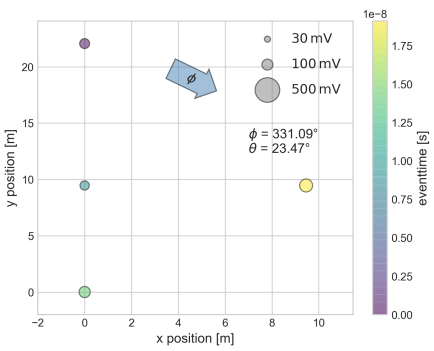

(d) Event 26

Figure 3.13: Exemplary events for the air shower array with the reconstructed shower direction shown in the plots.

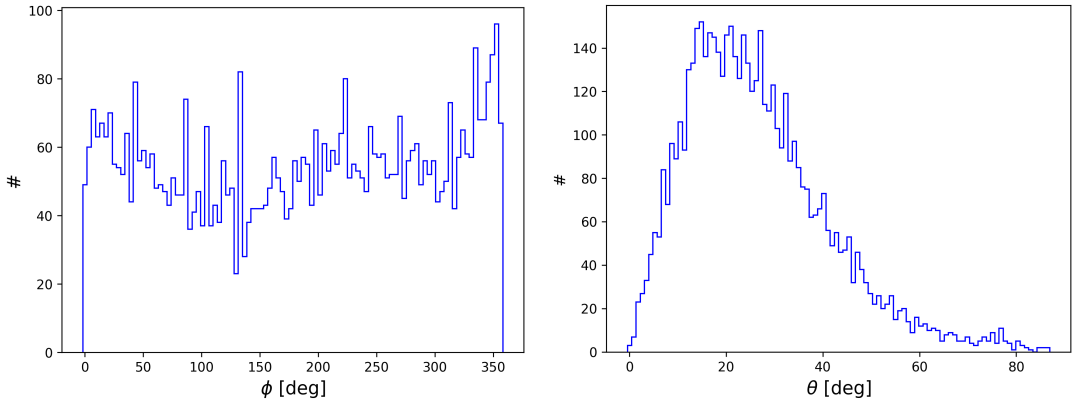

(a) azimuth angle ϕ distribution **(b)** zenith angle θ distribution

Figure 3.14: Angle distribution for the zenith and azimuthal angle.

In Figure 3.14 the distributions on the angles ϕ and θ are shown. As expected the azimuthal angle ϕ is distributed uniformly between 0° and 360°. The zenith angle is distributed between 0° and 90° and has its maximum around 20°. Usually one would suspect that the maximum should be at 0°, which is true if the distribution is normed on the solid angle $\Omega = 2\pi \cdot (1 - \cos\frac{\theta}{2})$. The bins are normed by $\Delta\Omega$ whereat θ_1 and θ_2 are the lower and upper boarder of one bin as described in Figure 3.15 and equation 3.8. The solid angle describes the area on a sphere with θ and ϕ as borders. If one norms an angle like the zenith angle on the solid angle the different sized surfaces are evened out [16].

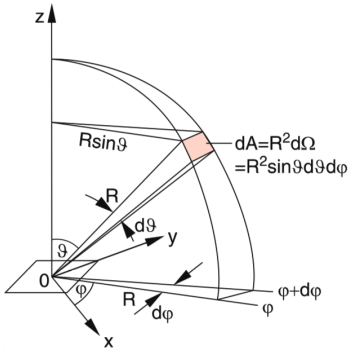

Figure 3.15: The solid angle $d\Omega = \frac{dA}{R^2} = \sin(\theta) \cdot d\theta \cdot d\phi$ [16].

$$\begin{aligned} d\Omega &= \frac{dA}{R^2} = \sin(\theta) \cdot d\theta \cdot d\phi \\ \implies \Delta\Omega &= 2\pi \cdot \big(-\cos\frac{\theta_2}{2} + \cos\frac{\theta_1}{2} \big) \end{aligned} \tag{3.8}$$

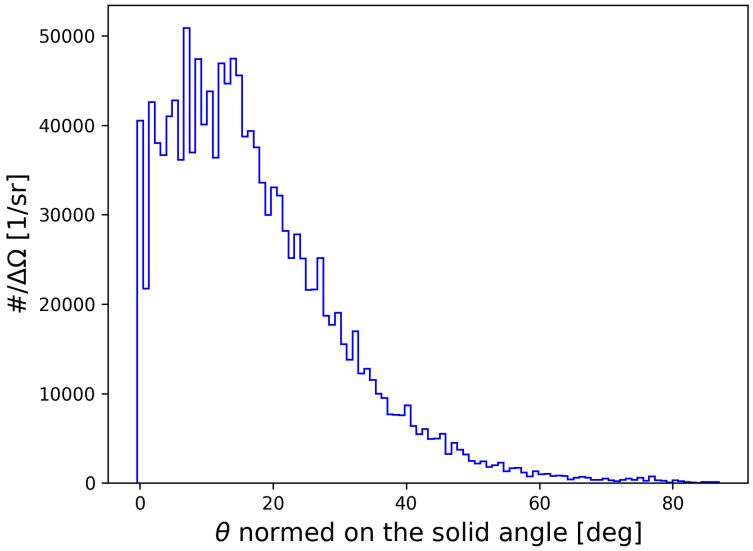

Figure 3.16: The solid angle $\Delta\Omega = 2\pi \cdot \left(-\cos\frac{\theta_2}{2} + \cos\frac{\theta_1}{2} \right)$ normalized zenith angle θ and its distribution.

To get a better idea on the shower direction, the azimuthal and zenith angles were combined into a polar histogram (Figure 3.17). Here again θ is not normed on the solid angle so more showers origin at around $\theta = 20°$ instead of $\theta = 0°$. The normed polar histogram looks as expected, as shown in Figure 3.18.

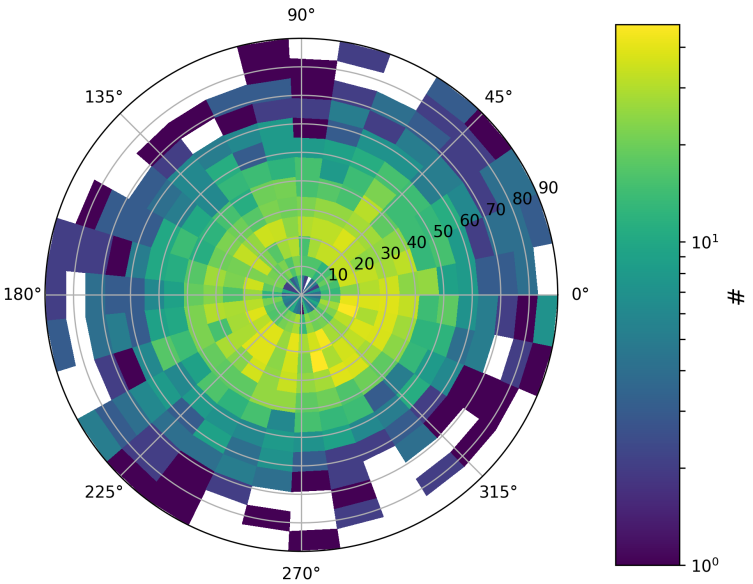

Figure 3.17: Polar histogram for the zenith and azimuthal angles θ and ϕ. This two dimensional histogram visualises the correlation between both angles and shows in which direction most showers arrive.

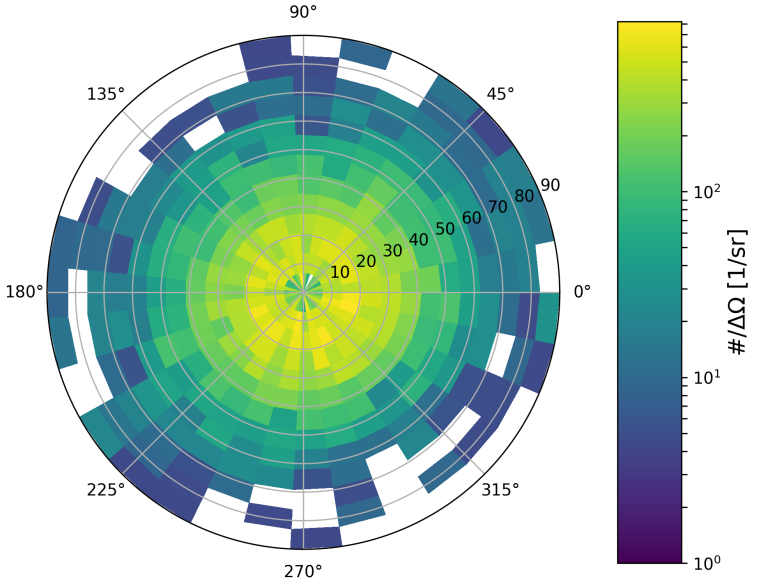

Figure 3.18: Polar histogram for the zenith and azimuthal angles θ and ϕ normed on the solid angle $\Delta\Omega = 2\pi \cdot \left(-\cos\frac{\theta_2}{2} + \cos\frac{\theta_1}{2} \right)$.

As seen in Figure 3.18 the showers distribute uniformly over the azimuthal angle. Also, most showers arrive under a low zenith angle. The flattening of the zenith distribution is explained by comparing the thickness of the atmosphere the particles in the air showers have to cross. Under a zenith angle of $\theta = 0°$ the distance within the atmosphere is the shortest and for $\theta = 90°$ it is the longest. The more time an air shower spends in the atmosphere, the more energy the shower will lose. For a longer route within the atmosphere the shower has a higher chance to not have enough energy left to reach the surface. Showers with a high zenith angle probably had a primary particle with a high energy. Additionally, particles with a high zenith angle have to pass more atmosphere near the surface where the density is higher. This results in a lower mean free pass and a higher loss of energy.

4

FAMOUS

FAMOUS ("First Auger Multi pixel photon counter camera for the Observation of Ultra-high-energy-cosmic-ray air Showers"), shown in Figure 4.1, is a compact imaging air-Cherenkov telescope originally developed for fluorescence light detection and now mainly triggers on Cherekov light [17]. This imaging air-Cherenkov telescopes (IACT) was first developed by the Auger experiment working group at the RWTH Aachen

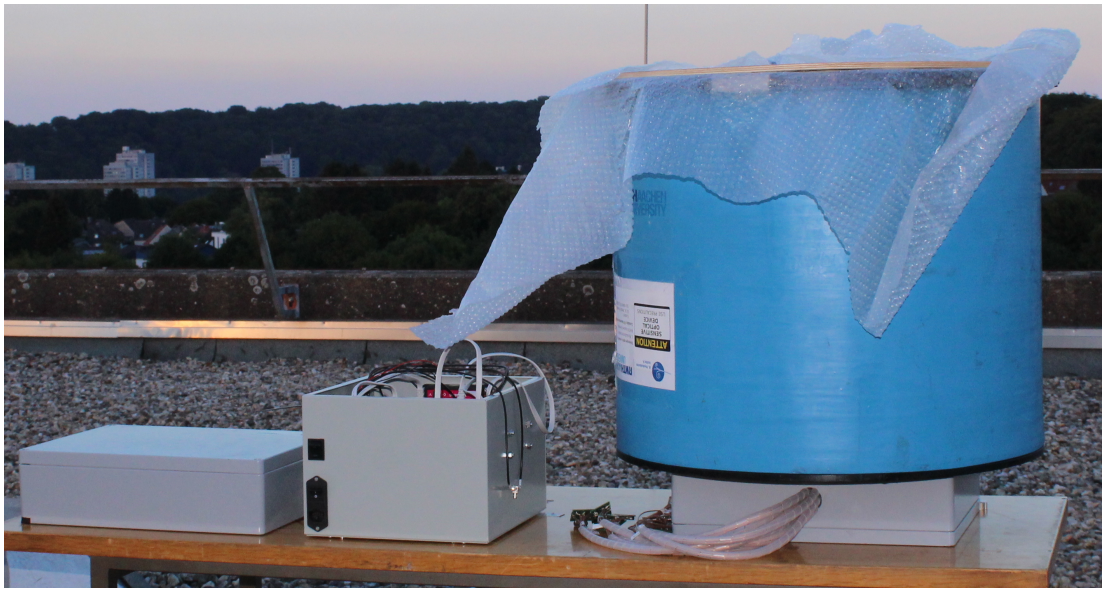

Figure 4.1: Picture of FAMOUS. On the left in the picture is the power supply and in the middle one can see the DAQ with the triggering system. In the box underneath the tube contains the electronics for the camera.

University as a SiPM based fluorescence telescope [10]. Low costs and a robust and small design gives the telescope a number of applications, for example in the Pierre Auger Observatory as AugerNext [18] or as part of a hybrid Cherenkov detector in a coincidence measurement as HAWC's Eye [10]. At the moment, there is a project running with FAMOUS as a surface extension for IceCube, called IceACT [9].

In the following chapter the data acquisition (DAQ), functions and measuring results for FAMOUS are outlined. More information on the setup and electrical components are in [9].

4.1 Setup and DAQ system of FAMOUS

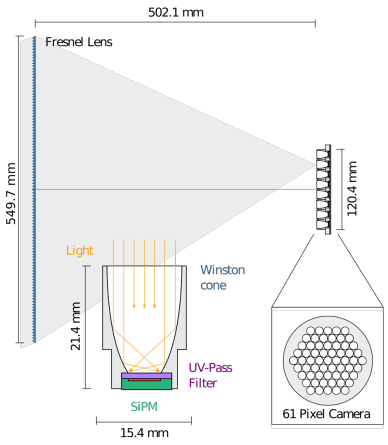

Figure 4.2: An overview on the optical setup of FAMOUS [9].

The main components of FAMOUS are the Fresnel lens with a diameter of $\varnothing = 549.7$ mm and a focal length of $f = 502.1$ mm, the Winston cones and the 6×6 mm^2 photo sensors. The telescope is designed to measure fluorescence light with a wide field of view of 12° (≈ 0.21 in radians) and the DAQ with GHz sampling speed is ideal for Cherenkov light detection.

The composure of the telescope is visualised in Figure 4.3 and the corresponding optical concept is shown in Figure 4.2. The camera consists of 61 active pixels built up out of a Winston cone and a SiPM as a photo sensor with a field of view of 1.5° each.

The SiPM based camera has temperature sensors which automatically compensate for the temperature dependency of the SiPMs. It is connected to a Power Supply Unit controlling the bias underneath the telescope.

The UV-optimized SiPMs are chosen for their photo detection efficiencies near the UV light spectrum due to the p-on-n silicon process. These wavelength include the typical Cherenkov spectrum. This allows the telescope to operate on rather bright nights as well, e.g. on moonlit nights [9].

In Figure 4.4, the FAMOUS electronics and data acquisition are shown in a simplified diagram. The SiPMs get the bias voltage from the power supply unit while sending the raw signals to the DAQ system. The signal is amplified in the amplifier and it is sent to the trigger master unit as well as to the digitizer. The digitizer returns a digital signal to the trigger master which masters the triggering signals and returns the data signals for them to be recorded on the PC.

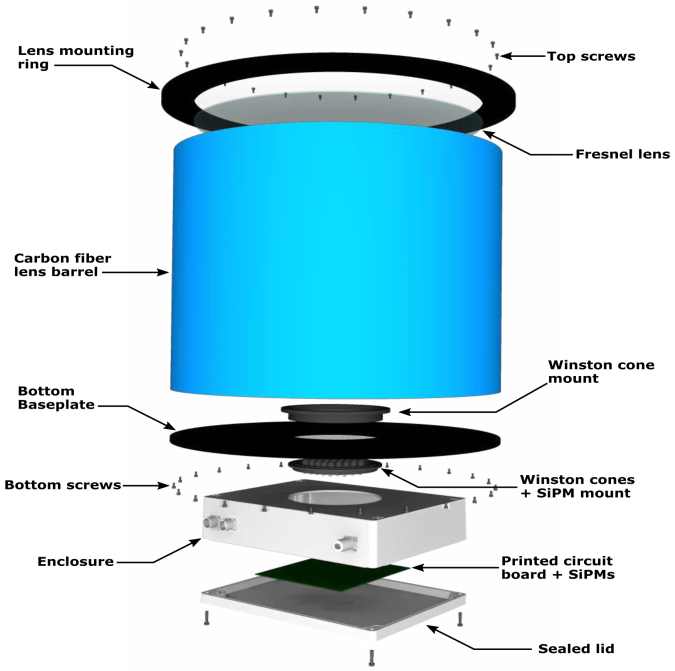

Figure 4.3: Mechanical assembly of FAMOUS showing the components within the telescope [9].

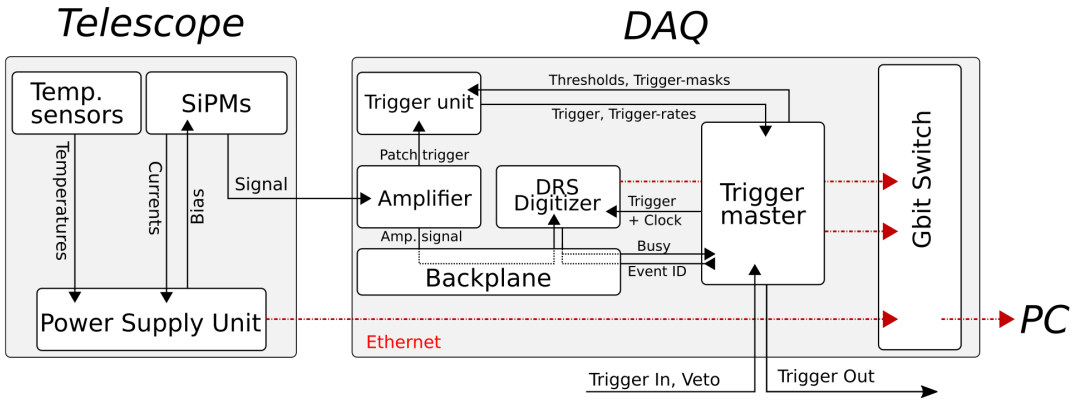

Figure 4.4: Schematic visualisation of the FAMOUS electronics. The SiPMs, bias control and temperature sensores are incorporated in the telescope enclosure. The Amplifier (FACT Preamlifier boards, FPA) amplifyes the originals SiPM signals. Afterwards the signals are distributed to the Trigger unit (FACT trigger unit, FTU) and to the Digitizer (FACT analog to digital, FAD). The Trigger master (miniFTM) takes care of clock and trigger distribution as well as the busy vetoing. The modules are conected by an integrated highspeed ethernet switch [9].

The signal path is visualised in Figure 4.5. The electronics are based on the First G-APD Cherenkov Telescope (FACT) system. The pre-amplifier board consists of 36 channels. It amplifies the signals which get led to the digitizer on the data-acquisition

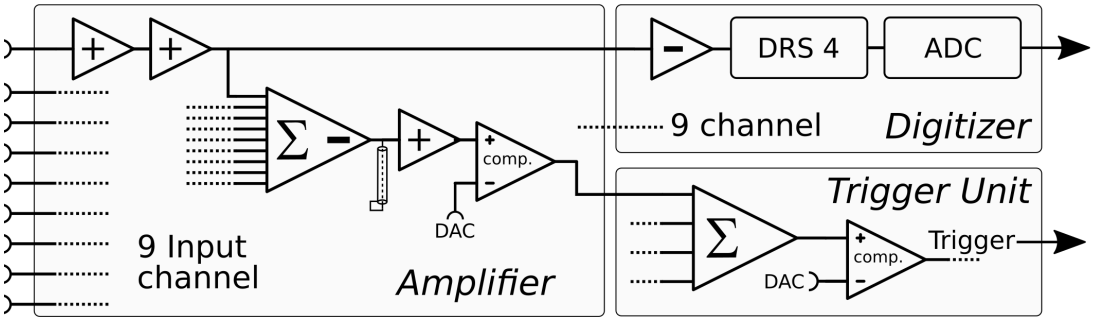

Figure 4.5: A simplified schematic sketch of the signal path from the sensors (on the left) to the data acquisition including the Trigger master [9].

board. The amplifier creates analog sums of four groups of nine channels each as well. The sums enter a discriminator followed by the triggering unit returning a primitive triggering signal which is led to the trigger master. The data acquisition board is based on DRS4 chips (Domino Ring Sampler) which are switched capacitor arrays with 9 channels and 1024 storage cells per channel storing the waveforms in a ring buffer. Here the analog amplified signals are buffered and led to a digitizer (analog-to-digital converter chips). Afterwards, the signals are progressed by a field programmable gate array (FPGA). Triggered events are tagged via a RS485 bus. The modules are plugged in a back plane, routing the pre-amplified analog signals to the data acquisition boards. The three boards per module are seen in Figure 4.6c [19, 9].

For more information on the DAQ system and the setup, check [9] and [19]. For this experiment the triggering mechanism is relevant and further explained in the following.

4.1.1 Triggering mechanisms for FAMOUS events

The camera is divided into eight trigger groups known as patches of up to nine pixels each by the adapter board (Fig. 4.6b), as seen in Figure 4.6a. Seven patches consist of nine pixels each, and can be marked as triggered if the summed up signal passes a digitally adjustable threshold. If the configurable number of patches is exceeded the telescope is triggered and saves the data for the event. The threshold voltage and the number of patches that have to be triggered is variable and can be changed in the system software, which is explained further in [9].

The three pixels in the corners are so called blind pixels. They make up the eighth patch which does not contribute to the triggering process. The blind pixels are pixels covered used as control pixels (e.g. for electronic noise).

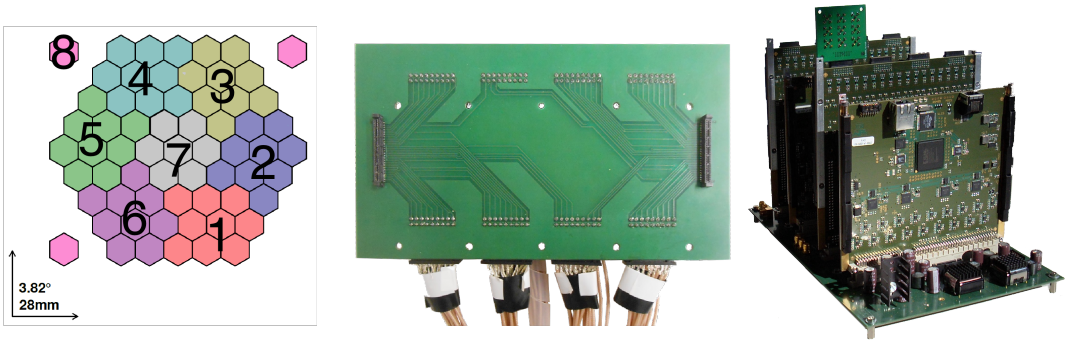

(a) Eight trigger patches. **(b)** Adapter board. **(c)** DAQ module.

Figure 4.6: a) Layout of the trigger geometry. Seven patches with nine active pixels each and one patch with three blind pixels. The last patch is excluded from the triggering system. Adapted from [9]. b) Adapter module for the virtual division of the camera into different trigger groups [9]. c) One module is made up of three boards to build the DAQ. The back plane hosts two pre-amplifier boards and two digitizer boards [9].

4.2 Event analysis and reconstruction

The reconstruction programs are from [20] with the common Hillas parametrisation [21]. The shown events and the discussed measurement are from June 26^{th} 2018 with 1741 triggering signals.

In Figure 4.7, an exemplary event is shown. For the reconstruction of the events the Hillas parametrisation is used [20, 21]. For this the shower image is approximated as an ellipse with the width (w) and length (l). Other classic Hillas parameters used for this reconstruction are the Center of Gravity (CoG) describing the Center of Gravity of the light distribution detected by the telescope and δ describing the angle between the image axis of the ellipse and the chosen x-axis from FAMOUS. Another semi-classic Hillas parameter used for the event reconstruction is the area A, naming the amount of pixels being part of the shower after image cleaning [20, 21].

For the evaluation of the recorded events, one looks at all pixels with a signal above an adjustable threshold. The threshold is computed with samples 10 to 50 for each pixel, whereat the level is calculated for each event. If a signal for one pixel exceeds the level it is treated as a hit pixel, the amount of the hit pixels equals the area. By stating a minimal area high noise signals are excluded as an event. With the reconstruction program and events with an area of at least three pixels, FAMOUS detected 121 events.

For the event reconstruction, the disp method in first approximation is used, as described by equation 4.1. The constant c from the formula was roughly approximated as $-5° \pm 1°$ for events with an area of at least three pixels [22].

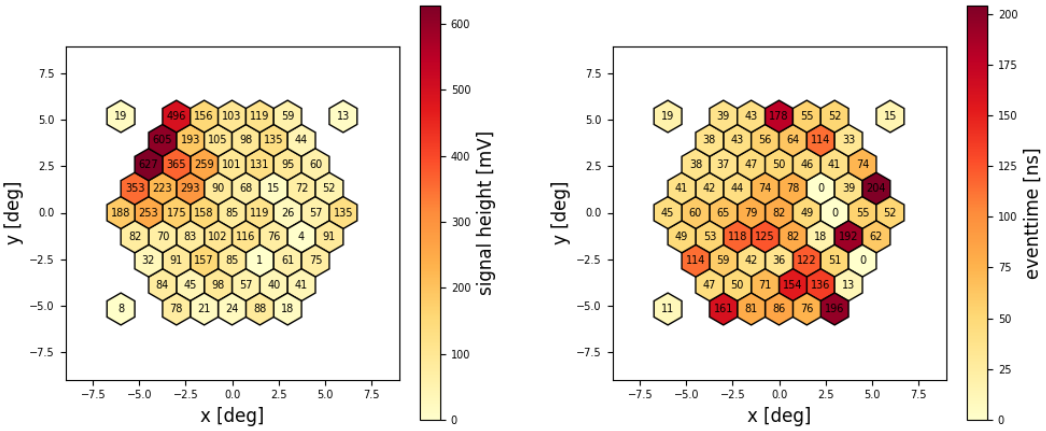

(a) Voltage **(b)** Time stamps

Figure 4.7: A FAMOUS event form the measurement of June 20^{th}. Hit pixels in Figure a) are hit during a small time period.

$$
\begin{aligned}
x_{angles,deg} &= x_{CoG} + \cos(\delta) \cdot c \cdot (1 - \frac{w}{L}) \\
y_{angles,deg} &= y_{CoG} + \sin(\delta) \cdot c \cdot (1 - \frac{w}{L}) \\
\theta &= \arcsin \sqrt{x^2_{angles,rad} + y^2_{angles,rad}} \\
\phi &= \arctan 2(y_{angles,rad}, x_{angles,rad})
\end{aligned}
\tag{4.1}
$$

For the event in Figure 4.7, the reconstruction of the shower direction leads to the azimuthal angle[1] $\phi = 123°$ and the zenith angle $\theta = 5.2°$. This event has an area of 12 pixels, the approximated ellipse a width of 1.06°, a length of 1.73° and $\delta = -1.9831$. In Figures 4.8 to 4.10 other reconstructed events are shown.

In Figure 4.11, the uniformly distributed azimuthal angle is expected. For the zenith angle, a rising slope is expected, since it is not normalized on the solid angle (this is shown in Figure 4.12) and the field of view for FAMOUS is at 12°, which is too low for the angle to decrease again. Both distributions are as expected but it is of importance to keep the low statistic of 121 reconstructed events in mind.

To get a clearer comprehension on the reconstructed shower direction one can take a look at Figures 4.13 and 4.14 where the distributions on the azimuthal and zenith angles are combined in a polar histogram. For the second figure (Fig. 4.14) the zenith angle θ is normed on the solid angle as seen in Figure 4.12.

[1]The calculated azimuthal angle describes the shower direction within the FAMOUS coordinate system. The FAMOUS coordinate system is indicated in Figure 4.7, the layout of the pixels in relation to the outside of FAMOUS has to be measured.

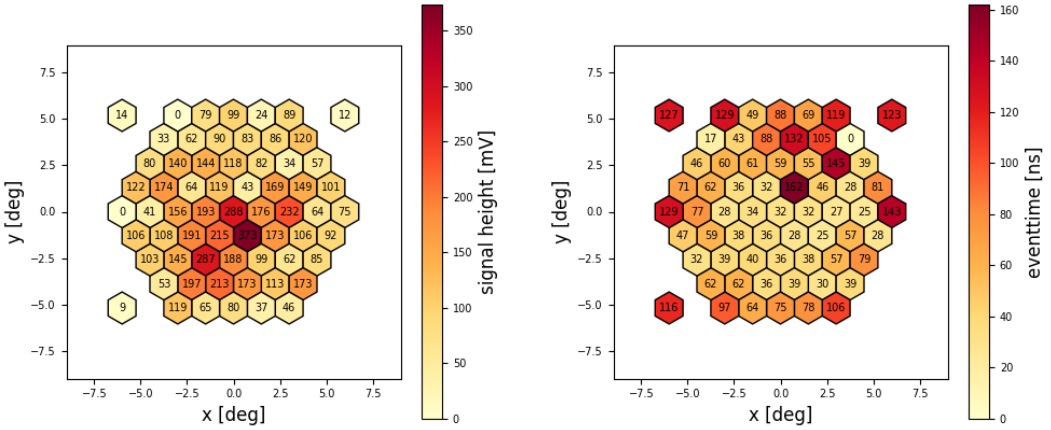

(a) Voltage **(b)** Time stamps

Figure 4.8: FAMOUS event from the measurement of June 20^{th}. With an azimuthal angle of $\phi = -105°$ and a zenith angle of $\theta = 0.3°$. The area is 9 pixels and the ellipse has a width of 0.99°, a length of 1.46° and $\delta = -2.0036$.

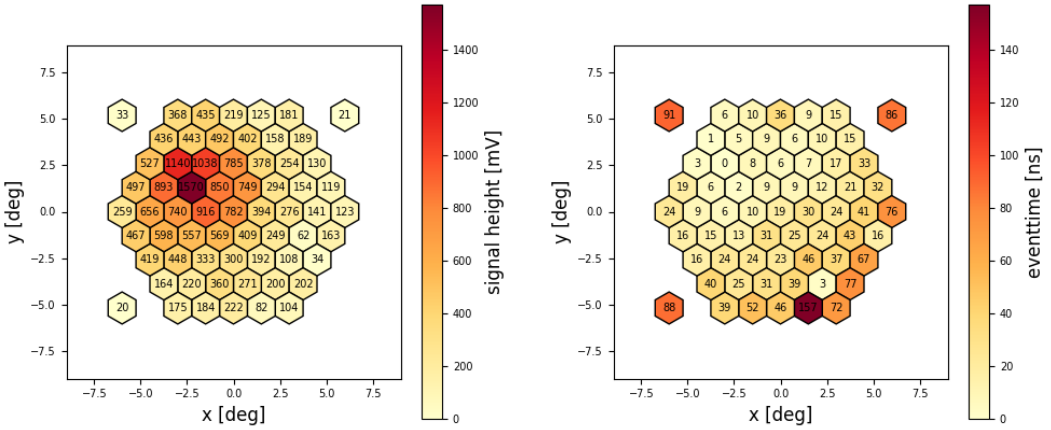

(a) Voltage **(b)** Time stamps

Figure 4.9: FAMOUS event from the measurement of June 20^{th}. With an azimuthal angle of $\phi = 143.35°$ and a zenith angle of $\theta = 1.95°$. The area is 46 pixels and the ellipse has a width of 2.25°, a length of 2.47° and $\delta = -1.456$.

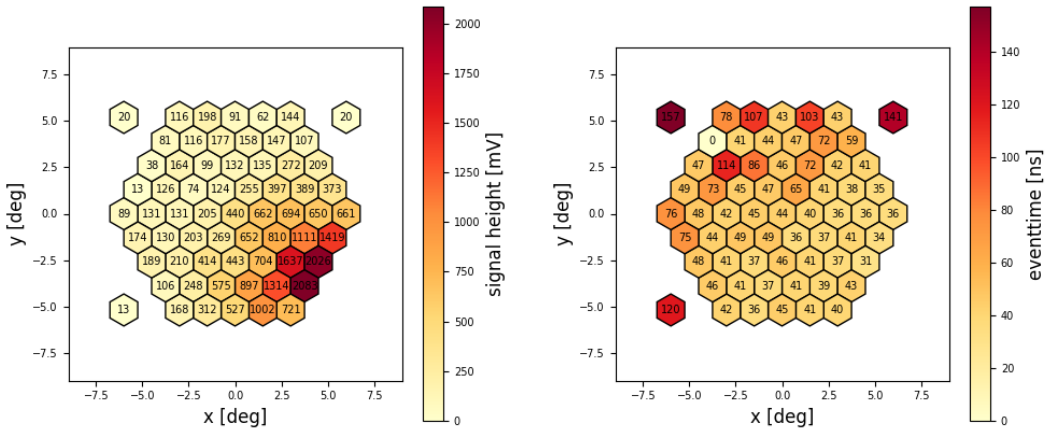

(a) Voltage **(b)** Time stamps

Figure 4.10: FAMOUS event from the measurement of June 20^{th}. With an azimuthal angle of $\phi = -40°$ and a zenith angle of $\theta = 2.9°$. The area is 51 pixels and the ellipse has a width of 2.42°, a length of 2.51° and $\delta = 2.8882$.

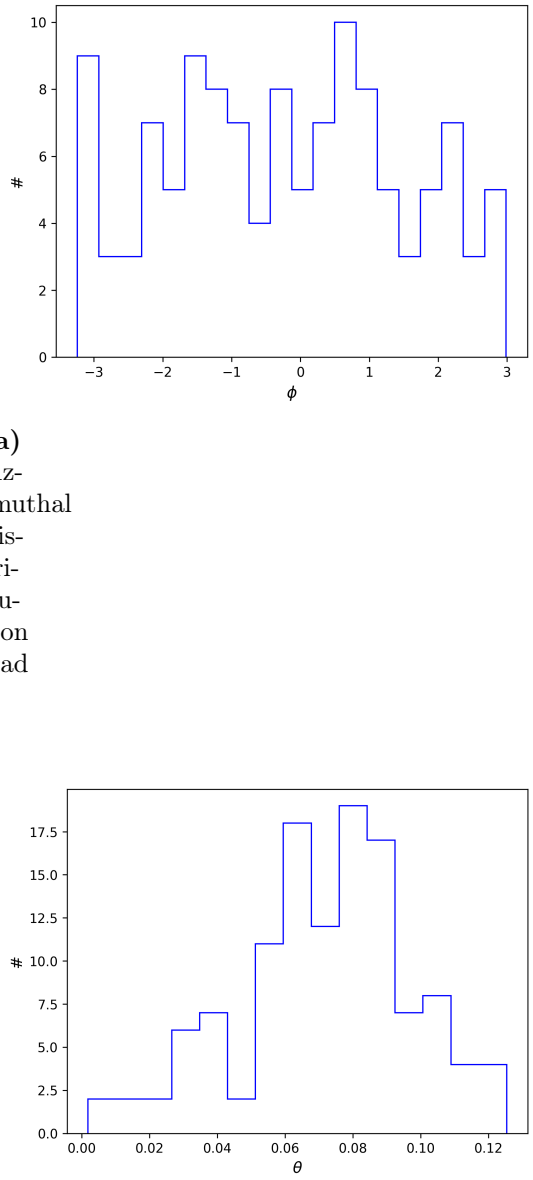

]
(a) Azimuthal distribution [rad

]
(b) Distribution of the zenith angle [rad

Figure 4.11: Distributions of the azimuthal ϕ and zenith θ angles for 121 events.

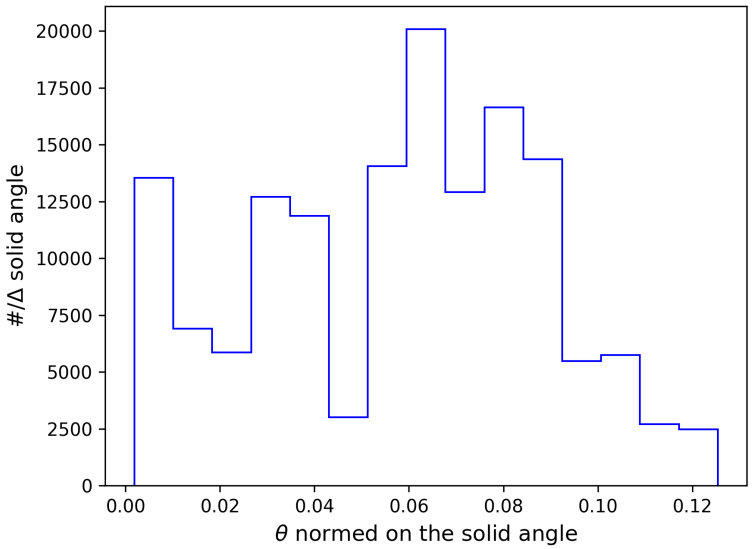

Figure 4.12: Distribution of the zenith angle θ normalized on the solid angle $\Delta\Omega = 2\pi \cdot \left(-\cos\frac{\theta_2}{2} + \cos\frac{\theta_1}{2} \right)$ whereat θ_1 and θ_2 are the edges for the corresponding bin. Further explained for Figure 3.16 for the air shower array. [rad]

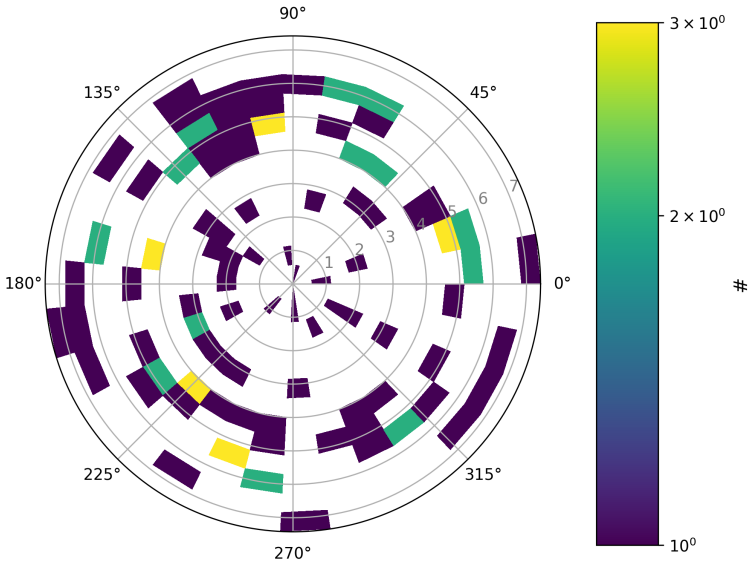

Figure 4.13: Polar histogram for the azimuthal and zenith distributions of the measurement with FAMOUS on the 26*th* of June.

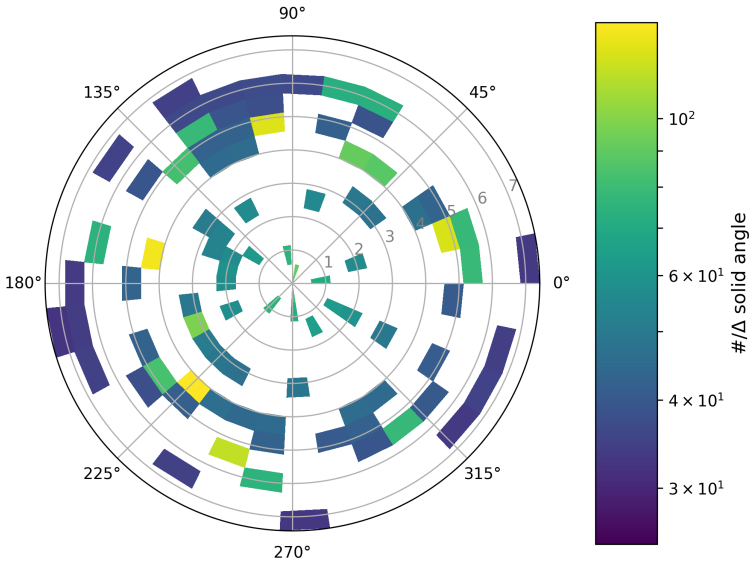

Figure 4.14: Polar histogram with the zenith angle normalized on the solid angle $\Delta\Omega$ as seen in Figure 4.12.

5

Setup of the hybrid air shower detector

There are multiple setups possible for the hybrid air shower consisting of the telescope FAMOUS and the SiPM based air shower array on the roof of the Physikzentrum. During the measurements, discussed in this thesis, two different methods where used as explained in this chapter.

In general FAMOUS can be triggered by the air shower array and vice versa. Alternatively both detectors can be triggered by their own triggering mechanisms while at least one triggering signal is flagged and saved with the events. This chapter discusses only the two methods of FAMOUS being triggered by the array and the array flagging the triggering signals from FAMOUS in detail, since these are the ones which were used, since they are the easiest to realize and the most reasonable. The other methods are not reasonable since the rate for FAMOUS is very high, which would result in lots of events and in most the array would not see anything, making it a high number of datapoints to work with, without any apparent advantages. On the other hand FAMOUS has no easy way to record the triggering signal from the array. This is the reason the telescope did not flag the array triggering signal.

For all setups FAMOUS was placed on the roof next to detector 3. With this setup the showers are expected to have a low zenith angle for FAMOUS and the array to detect it.

5.1 Triggering FAMOUS with the air shower array

During this setup, FAMOUS was triggered externally by the air shower array. This way one can compare what FAMOUS detects while a shower passes trough the array. It

Figure 5.1: Setup of the coincidence measurement on the roof of the Physikzentrum.

allows an easy comparison between the events but the rate of events in general is rather low. With this setup the events from the array and the telescope can be matched easier since the rate is lower and both are triggered by the same signal with a small delay.

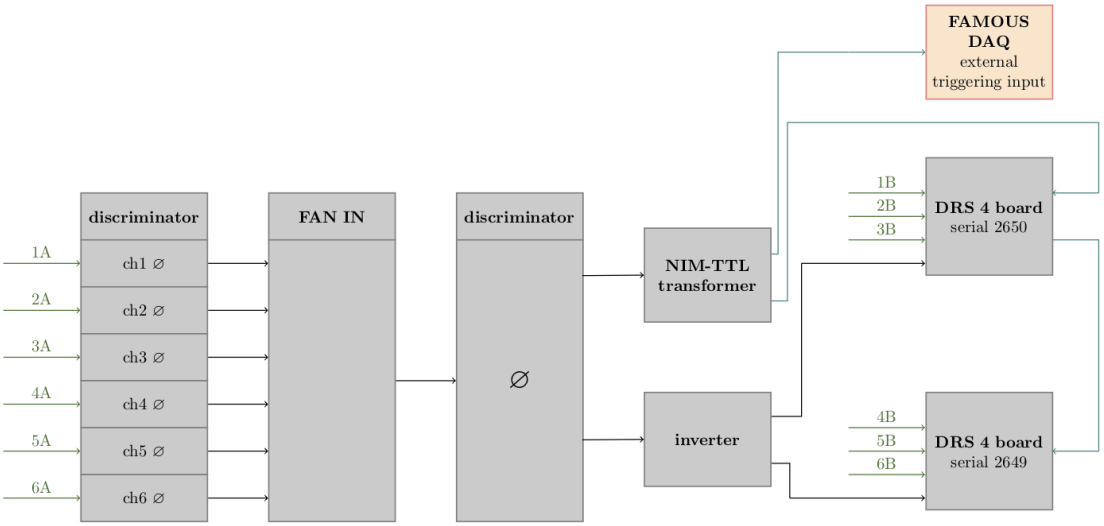

Figure 5.2: Schematic visualisation of the setup: Triggering FAMOUS with the array.

As shown in Figure 5.2, the triggering signal from the inverter led to the DRS4 boards is doubled by using a second output from the summed discriminated signal and leading it to another NIM-TTL-transformer. The TTL-triggering-signal is led from the triggering modules outside into the triggering system from FAMOUS. This generates a delay of approximately 185 ns[1]. This delay is within an allowed time window, since the telescope buffers enough samples to record the triggered events.

[1]The delay of the 30m long cable leading the signal to the telescope was measured with an oscilloscope as $t_{delay} = (167 \pm 3)$ ns. The signal was led through two shorter cables, these delays where estimated as 10 ns and $3 - 4$ ns (this was not measured but given on the cable label or estimated with the cable length).

5.2 Flagging FAMOUS' trigger with the air shower array

For the second setup both, the array and FAMOUS, where triggered with their own triggering logic. To record which events appeared in coincidence detector 6 is detached from the array[2] and the triggering signal from FAMOUS was recorded instead. The triggering signal was led with the same cables as described before with a signal delay of ≈ 185 ns. The signal can be seen during the last 200 ns of the sampling.

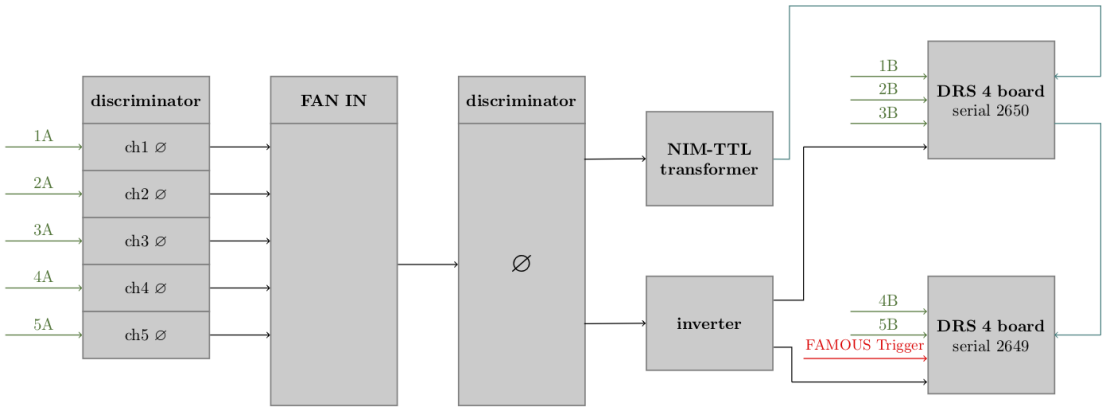

Figure 5.3: Schematic visualisation of the setup: Flagging FAMOUS' triggering signal.

[2]Detector 6 is not recorded by the DRS4 boards and has no input into the triggering signals. This means the array only has five detectors to measure events. The triggering modules (seen in 5.3) are setup analogue to the triggering system with six detectors.

6

Measuring in coincidence with FAMOUS and the air shower array

For measurements with FAMOUS and the air shower array in coincidence, the night should have no clouds and it should be a new moon, since the telescope is sensible to night sky background. Alternatively, the moon has to stay at a low angle, so the camera in FAMOUS is not saturated.

During the time of this thesis there where three measuring nights with different cloud conditions and the moon was at different states within the lunar cycle. During every measurement, it was never night, which means, that it was the darkest during the astronomical twilight [23]. The weather and state of the lunar cycle during the measurement is relevant to the results, since the telescope threshold and triggering rates are dependent on it.

Measurements on June 20^{th} 2018

The first night of measurements was to test the setup and check the rates and delays between the detectors. It started around 11.20 pm [1], with two measurements of FAMOUS being triggered by the array. These measurements did not start and end simultaneously. This has to be taken into account while matching the events.

Afterwards, a longer measurement with the array flagging FAMOUS' triggering signal started at 00:05 am. Around 1:00 am the array recording was stopped briefly to check

[1] The starting time defined as the starting time of the measurement with the array. One has to regard the time offset from the computer saving these time stamps, which can change between different measuring days and will be calculated later on.

on the triggering flag and around 1:35 am the measurement was stopped due to a cloud scattering light and saturating the camera in the telescope.

The night had a few clouds at the horizon, which mostly did not influence the telescope. The moon passed the local meridian at 7:58 pm with 41.3° above the horizon. It set at 2:17 am which means, it was probably too low to influence the results with the telescope [23].

Measurements on June 26^{th} 2018

During the second night of measurements, only the second setup described in section 5.2 where recorded. This means the array flagged the FAMOUS' trigger during all recordings and the telescope was never triggered by the array. The first recording in coincidence started at 00:59 am. The array measurement was paused shortly at 1:39 am to check for the FAMOUS' triggering flag. FAMOUS recorded data in runs of 5 minutes each and adjusted the threshold voltage every run. Both measurements ended around 3:15 am.

The night sky was clear from clouds, the moon was almost fully illuminated[2] and passed the meridian at 00:39 am with 18.9° above the horizon [23]. The moon was above the horizon for the entire measurement, but staying low enough to not influence the telescope.

FAMOUS detected 1741 events during the whole measurement while the array detected 43 in the first and 119 events in the second half of the measurement. During the two measurements, 7 and 19 events in coincidence were detected respectively.

Measurements on July 13^{th} 2018

For the last measurement, the recording program of the air shower array was adjusted in a way that it not only saves the event time but also the corresponding microseconds[3].

The measurement started around 2:40 am with the array triggering the telescope. At 3:00 am the second measurement started with the FAMOUS trigger being flagged by the array.

The night started cloudy at the horizon but cleared up till the coincidence measurements started. The moon was not above the horizon during the measurements and was not illuminated[4] [23].

[2] On June 28^{th} was a full moon.

[3] The microseconds are jittery but are needed to match the events, see section 6.1. In that section the reason to change the time settings becomes apparent

[4] The eclipse was mid day on the 13^{th} of July.

6.1 Synchronizing of independent data sets

Since the time stamps for FAMOUS and array events are not the same but have a time difference[5] which has to be calculated to match the events in coincidence.

Therefore the average time difference between the array time stamp (t_i^{array}) of an event measured in coincidence and the closest FAMOUS time stamp ($t^{\text{FAMOUS,i}}$) was computed and the array timestamps where shifted by a factor k in order to get the minimal average time difference with k_0. If the array time stamps are shifted by k_0 they should match with the FAMOUS time stamps for events in coincidence.

$$\Delta t = \sum_i (t^{\text{FAMOUS},i} - (t_i^{\text{array}} + k)) \tag{6.1}$$

Measurements on the 20^{th} of June 2018

For the first night the time shift k_0 was calculated with both measurements at the beginning of the night, where the array triggered the telescope. With this method only events in coincidence were considered which makes the matching of events rather easy, although the measurements did not start at the same time which concludes in cutting some array events away as shown in Figure 6.1.

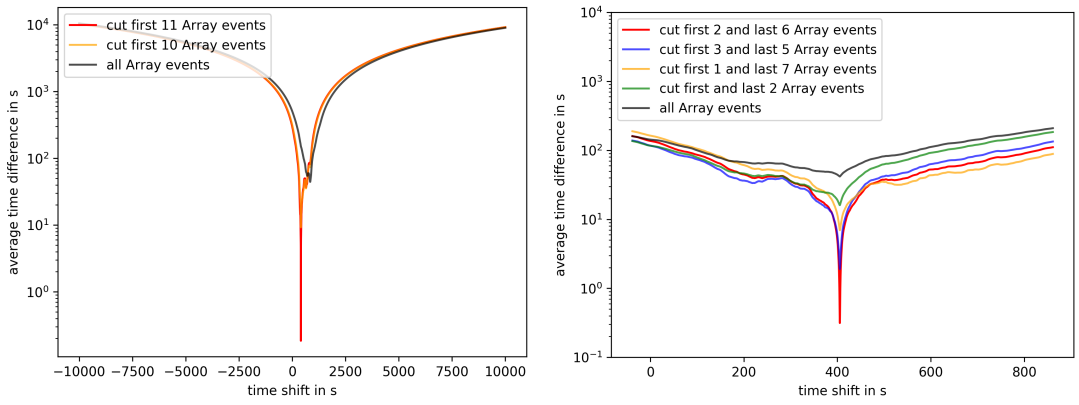

(a) 20Jn.A starting at 11:23 pm.

(b) 20Jn.B starting at 11:39 pm.

Figure 6.1: Visualisation of the average time difference between the array and FAMOUS timestamps dependent on the time shift k for the measurements on June 20^{th}.

[5]Especially for the first measurement the Computer with the array software had no access to the internet for more than half a year which led to a imprecise unixtime. But after the computer was connected to the internet and the clock could be tuned the timestamps did not match precisely, since the detectors run on different systems which reach different time imprecisions.

The minimization of equation 6.1 led to a time shift of $k_0^{20\text{Jn.A}} = 404.99$ s and $k_0^{20\text{Jn.B}} = 405.34$ s for the second measurement[6]. For the used time shift the mean was used for the further analysis, resulting in $k_0^{20\text{Jn}} = 405.17$ s.

Measurements on the 26^{th} of June 2018

Before the second night of measurements, the computer on the roof with the array control systems was connected with the internet, what leads to expect a time shift k_0 of a few seconds. Since no measurement of the array triggering the telescope was done, there are more events with FAMOUS than there are array events measured in coincidence[7]. This may lead to an imprecise calculation of the time stamp, especially if it is taken into account that the array time stamps are only precise in the order of one second.

The minimization of equation 6.1 led to a time shift of $k_0^{26\text{Jn.A}} = 2.70$ s and $k_0^{26\text{Jn.B}} = 2.80$ s for the second measurement. The calculation of these two time shifts were regarding all events. If only reconstructible FAMOUS' events were used, the minimum would be higher, since it is possible that events in coincidence where excluded of the calculation. Each calculated time shift was used to match the events from the corresponding measurement.

Measurements on the 13^{th} of July 2018

For the last measurement, the control program for the array was modified to save the milli- and microseconds with the timestamps for each event. This way, the time synchronisation should be more precise.

In the first measurement the air shower array triggered FAMOUS externally and in the second measurement the FAMOUS' triggering signal was flagged by the array. The variation of the time shift k is seen in Figure 6.3.

The ideal time shift for the first measurement was calculated to $k_0^{13\text{Jl.A}} = 27.22$ s and for the second measurement $k_0^{13\text{Jl.B}} = 27.45$ s resulted.

[6]The labels „20Jn.A "or „20Jn.B "are a method to label the different measurements. The first number is the day, „Jn"stands for June and „Jl"for July. The following letters name the run of the evening with the array (A: first run, B: second run).

[7]This is known due to the flag, that recorded the triggering signal from FAMOUS.

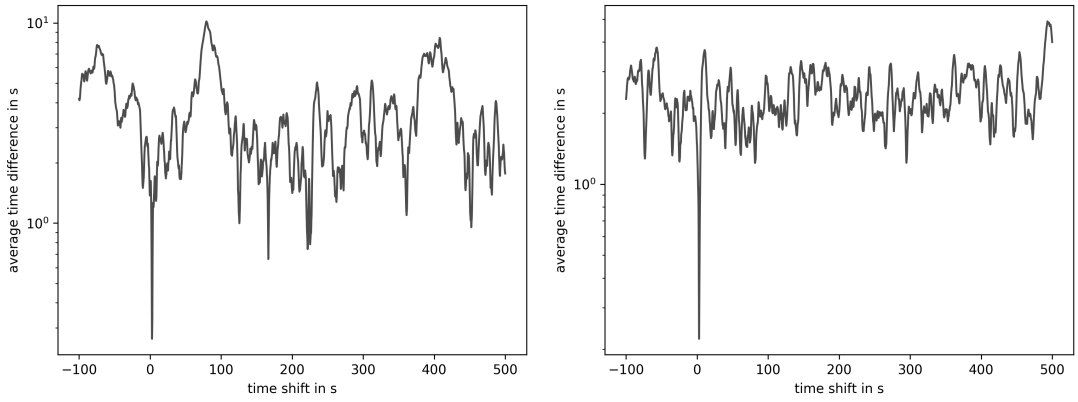

(a) 26Jn.A, starting at 00:59 am.

(b) 26Jn.B, starting at 1:39 am.

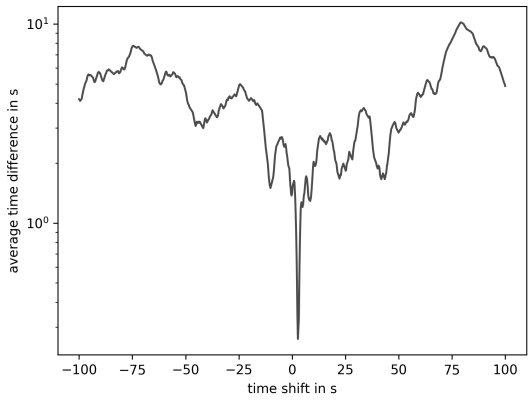

(c) 26Jn.A, zoom on the minimum.

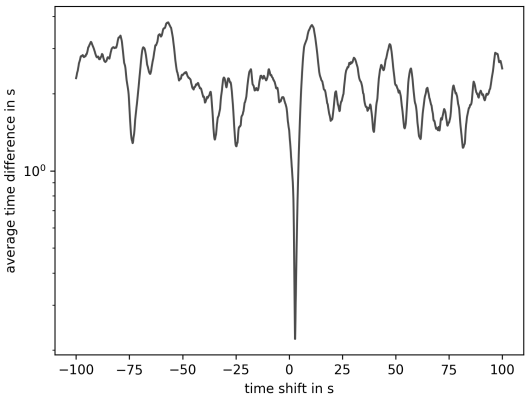

(d) 26Jn.B, zoom on the minimum.

Figure 6.2: The average time difference as a function of the time shift k. Plots a) and b) give an overview on where a minimum is and verifies if it is a clear minimum. Plots c) and d) show the precise minimums.

6.2 Data analysis

An event measured in coincidence is reconstructed if the array and the telescope could reconstruct the event separately. After the analysis of the events, 12 out of 69 events[8] in coincidence could be reconstructed.

[8]This number includes all measurements and also the coincidences during the measurements where the array triggered FAMOUS externally.

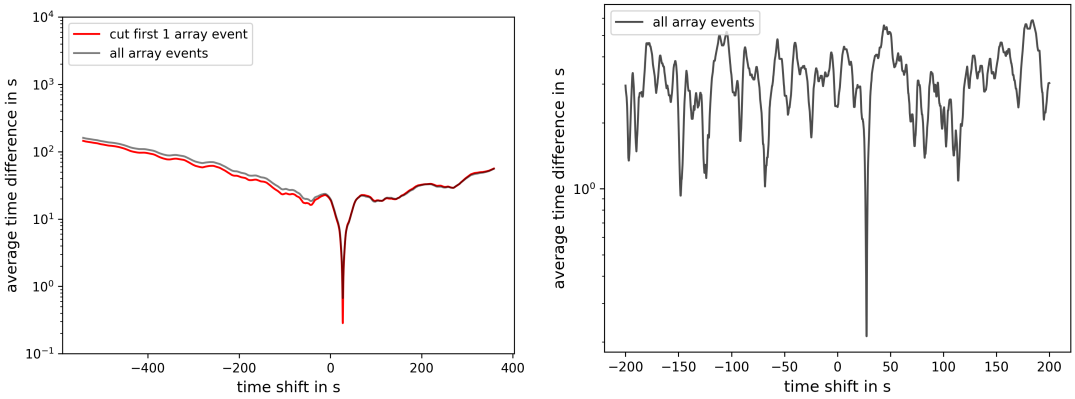

(a) 13Jl.A starting at 2:39 am. **(b)** 13Jl.B starting at 3:03 am.

Figure 6.3: Visualisation of the average time difference between the array and FAMOUS timestamps dependent on the time shift k for the measurements on July 13^{th}.

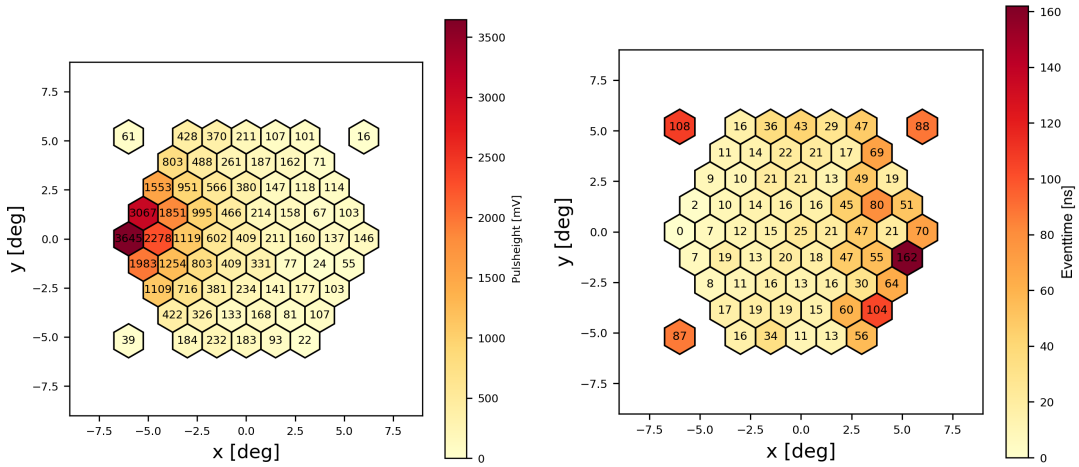

(a) Signal heights. **(b)** Timestamps.

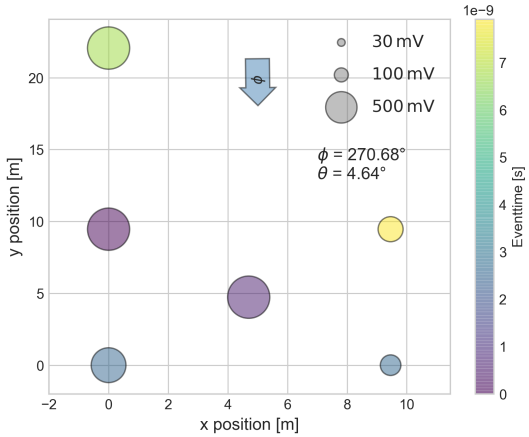

(c) Corresponding array event.

Figure 6.4: Event (A) in coincidence of the night of June 20^{th} 2018. A=46 pixels, l= 3.285°, w= 2.303°, $\delta = -2.6693$.

In Figure 6.4 an exemplary visualisation of an air shower hitting the air shower array and FAMOUS in coincidence. The event was detected during the measurements on the night of June 20^{th} at 11:42:47 pm and 170 ms (shifted array time stamp; FAMOUS time stamp: 11:42:47 pm and 307 ms). 46 pixels where triggered for FAMOUS and the event has a length of 3.285°, width of 2.303° and $\delta = -2.6693$.

Every detector in the air shower array triggered for the event and send out a high signal which indicates that the shower center was in the area of the air shower array.

The shower reconstructions resulted in the zenith angles $\theta_{array} = 4.64°$ and $\theta_{FAMOUS} = 3.26°$. The calculated azimuthal angles are $\phi_{array} = 270.68°$ and $\phi_{FAMOUS} = 0.57°$ however the azimuthal angles are not comparable since the angle for FAMOUS is in relation to the internal coordinate system and the angles for the air shower array is calculated in relation to north[9]. Additionally the uncertainties on the FAMOUS reconstruction is high since the event shows a lot of the hit pixels at the boarder of the camera which means the leakage of the event is high and with that the uncertainties are higher.

[9]One can determinate the orientation of the internal coordinate system from FAMOUS by illuminating one side with a laser. This was not prioritised in the thesis but will be done before a lab course with the telescope starts.

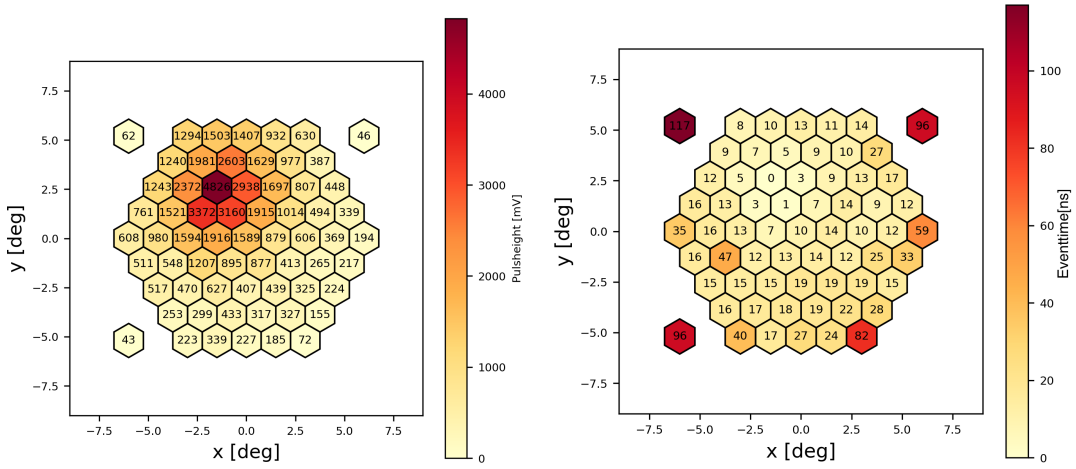

(a) Signal heights. **(b)** Timestamps.

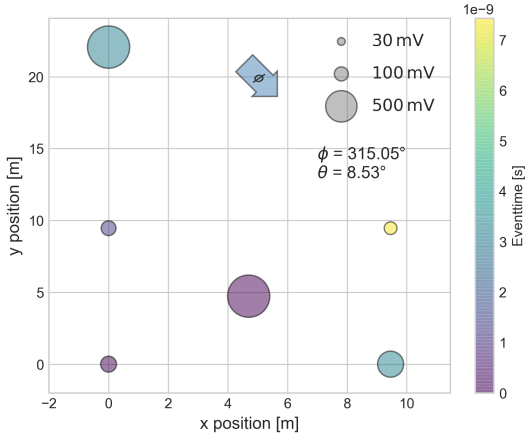

(c) Corresponding array event.

Figure 6.5: Event (C) in coincidence of the night of June 20^{th} 2018. A= 61 pixels, l= 2.447°, w= 2.391°, $\delta = -1.8707$.

The event seen in Figure 6.5 was detected at 11:49:08 pm and 340 ms (shifted array time stamp; FAMOUS time stamp: 11:49:08 pm and 621 ms). The shower direction reconstructions resulted in the zenith angles $\theta_{array} = 8.53°$ and $\theta_{FAMOUS} = 1.80°$ and the azimuthal angles $\phi_{array} = 315.05°$ and $\phi_{FAMOUS} = 116.88°$.

For the analysis, only the reconstructed events are regarded. In Table 6.1 the reconstructed events are listed with the reconstructed azimuthal ϕ and zenith θ angles from the telescope and the array, as well as the triggered area from FAMOUS and the detector multiplicity. The corresponding events can be found in the appendix.

For the further evaluation of the measurements in coincidence some correlation plots are created. The correlation between angles of the reconstructed events is difficult, since the array has a higher uncertainty due to its small size. Also the uncertainty

Date and event	θ_{FAMOUS}	ϕ_{FAMOUS}	area A	θ_{array}	ϕ_{array}	multiplicity
20.06.2018 A	3.26°	175.44°	46 pixels	4.64°	270.68°	6 detectors
20.06.2018 B	2.67°	37.99°	54 pixels	16.95°	153.91°	5 detectors
20.06.2018 C	1.80°	116.83°	61 pixels	8.53°	315.05°	6 detectors
20.06.2018 D	6.17°	−115.39°	5 pixels	11.94°	298.28°	5 detectors
20.06.2018 E	5.09°	−89.50°	4 pixels	16.60°	251.78°	4 detectors
20.06.2018 F	8.19°	60.00°	3 pixels	3.24°	93.18°	3 detectors
20.06.2018 G	5.16°	151.11°	4 pixels	17.14°	303.91°	3 detectors
26.06.2018 H	3.62°	26.57°	4 pixels	24.04°	340.22°	4 detectors
26.06.2018 I	4.59°	−102.95°	9 pixels	16.23°	153.22°	4 detectors
26.06.2018 J	4.90°	−90.65°	5 pixels	42.83°	303.28°	5 detectors
26.06.2018 K	6.06°	−108.65°	5 pixels	26.42°	273.54°	4 detectors
13.06.2018 L	6.09°	0.97°	5 pixels	8.39°	174.75°	3 detectors
13.06.2018 M	6.14°	−167.14°	5 pixels	9.10°	236.14°	3 detectors

Table 6.1: Overview of all events measured in coincidence.

on the FAMOUS angle reconstruction is high since it contains a constant c (equation 4.1) which has to be determinated in a more precise way with simulated data. These difficulties and uncertainties on the angles make the comparison less exact.

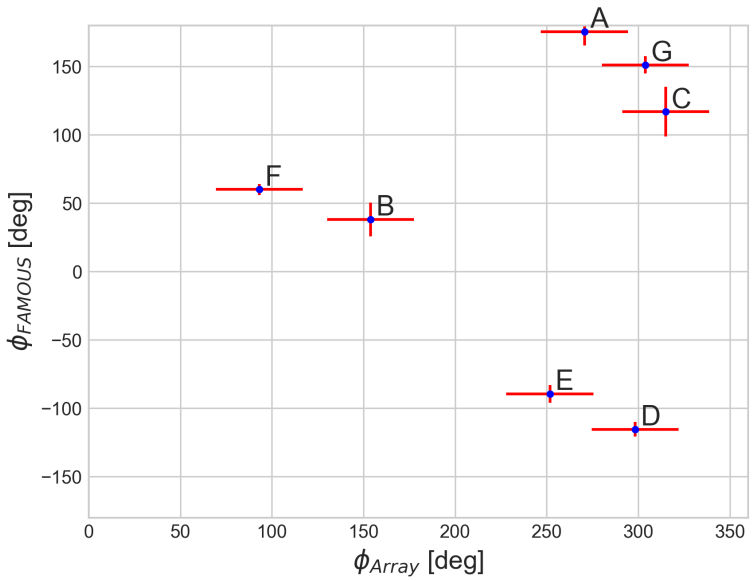

Figure 6.6: Correlation between the reconstruction with FAMOUS and with the air shower array for the azimuthal angel ϕ. The uncertainty on ϕ_{Array} is estimated as 24° due to the fluctuations within the air shower which have a high influence on the reconstruction with the array. The uncertainties on ϕ_{FAMOUS} are low in comparison. $\sigma_{\phi_{FAMOUS}}$ results from the propagation of uncertainty and is inversely proportional to the zenith angle θ_{FAMOUS}.

For the correlation between the azimuthal angles ϕ, one has to keep in mind that the orientation of the telescope changed between measurements, which is why only events

from the measurements on June 20*th* are regarded, in order to receive an accurate comparison. In this plot the reconstructed angles from the telescope are not in relation to north but in relation to the internal x-axis as explained in chapter 4. One can already surmise the correlation between the two angles. In a fit with $\phi_{FAMOUS} = -m \cdot \phi_{Array} + b$ it is expected to receive a slope of $m = -1$ and a difference between the two intercepts of $\Delta b = 360°$.

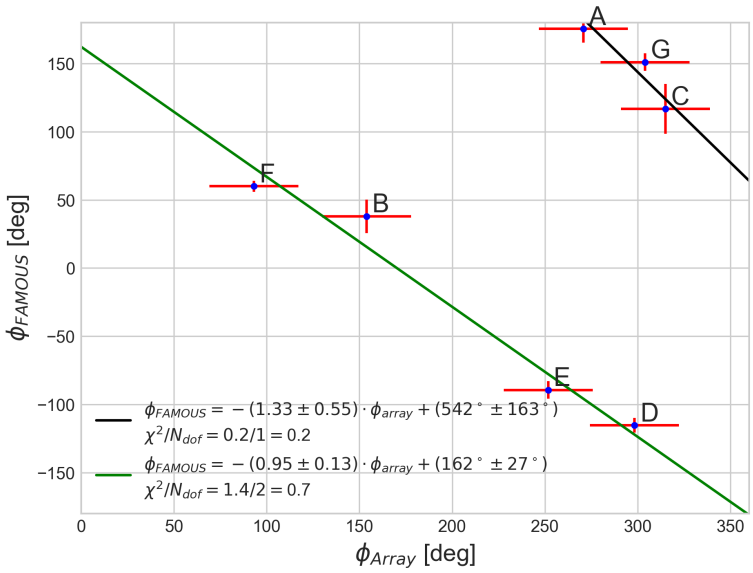

Figure 6.7: The correlation between both azimuthal angles has been visualised in this plot by fitting lines as $\phi_{FAMOUS} = -m \cdot \phi_{Array} + b$ trough the data points A, C and G (respective B, D, E, F).

As shown in Figure 6.7 the correlation between the azimuthal angles is clearly visible. The slope of both reconstructions is mutual with 1 which is expected since the detectors should reach the same reconstructions. The intercepts at $(542 \pm 163)°$ and $(162 \pm 27)°$ have a difference of $(380 \pm 164)°$ which is in agreeing with 360°.

The analysis in Figure 6.7 does not regard the fact that the lines need to match up and return on the other side of the circle. This is regarded in Figure 6.8. In this plot the slope was set to -1 and only the intercepts was fitted to the data point. As it can be seen the reconstructions seem to have systematics depending on the direction the shower arrives from. This can be discussed and confirmed during a further analysis of events measured with the hybrid air shower detector.

Another sign for the successful fits is the fact that the intercepts are similar within the uncertainties to from both fitting methods.

In Figure 6.9 the reconstructed zenith angles are shown. It can be seen, that most of the reconstructed angles with the array are not within the field of view from FAMOUS. This could have several reasons. The event matching could have assigned the wrong events to each other although this is rather unlikely, since the time differences are all below 0.6 seconds as seen in the appendix (Figures A.3, A.9 and A.14). Likelier the events

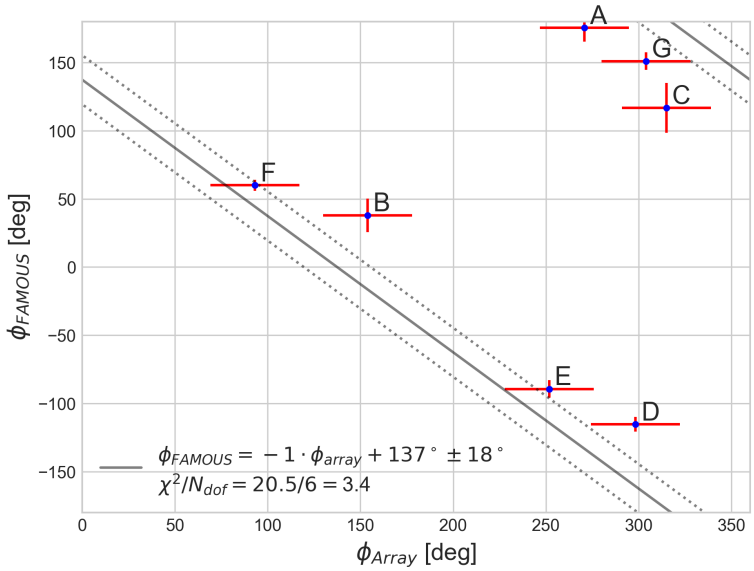

Figure 6.8: The correlation between both azimuthal angles has been visualised in this plot by fitting lines as $\phi_{FAMOUS} = -1 \cdot \phi_{Array} + b$ through all data points by shifting events A, C and G and receiving a line in a circle (mod360°).

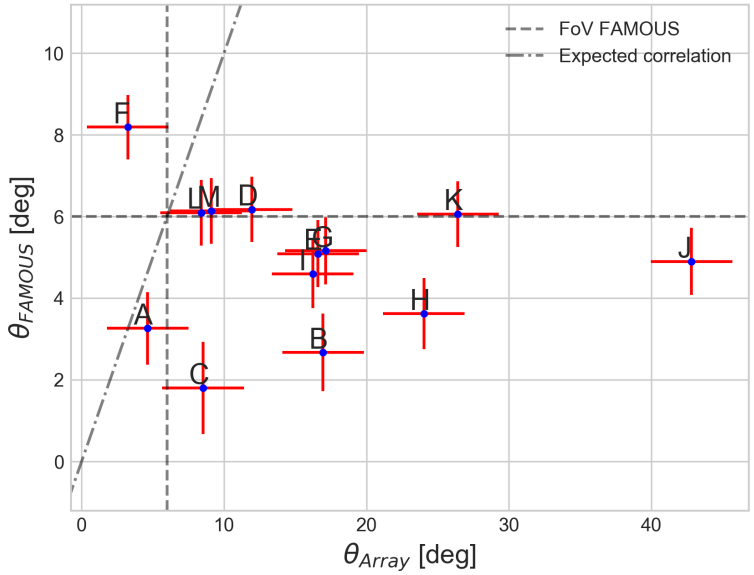

Figure 6.9: Correlation between the reconstructed zenith angle from FAMOUS and the air shower array. The dashdotted line symbolizes the expected correlation between the angles and the dashed lines mark the field of view from FAMOUS. The uncertainties are $\sigma_{Array} = 2.9°$ for vertical air showers and for σ_{FAMOUS} the hight of the uncertainty fluctuates slightly dependent on the zenith angle between 1° and 2°.

seen with FAMOUS only are subshowers and the big shower was missed in addition to a imprecise reconstruction with the array.

Events with a high leakage are expected to appeare closer to the limits of the field of view [24, 22]. As it can be seen in the plots for events L, M, D and K (in the appendix), these events have a high leakage. The leakage of the events E, G, I is not low either, which is confirmed with Figure 6.9. Event F is calculated not to be in the field of view with the Hillas parameters. That the reconstruction gives results larger than 6° for the zenith angle is possible due to the disp method[10]. As shown in Figure A.7 only three pixels are hit as part of the event. This and the fact that the event has a high leakage may result in an imprecise calculation of the zenith angle for this event.

The uncertainties on the zenith angle reconstructed by the array are $\sigma_{\theta_{array}} = \pm 2.9°$ as explained in chapter 3. In this work the errors were calculated by a variation of the detector positions and arrival times within their uncertainties. This does not include the fluctuations within the air shower which has a high impact on the shower direction due to the limited size of the air shower array.

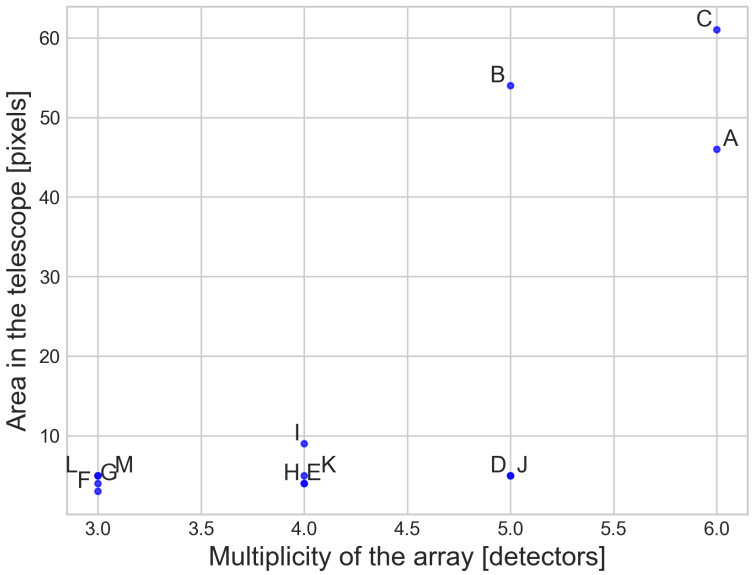

Figure 6.10: Correlation between the number of hit detectors in the array and the hit area within the telescope for events measured and reconstructed in coincidence.

In Figures 6.10 and 6.11, the brightness of the showers is shown. In Figure 6.10, the number of hit pixels is compared with the number of hit detectors and in Figure 6.11 the signal height in millivolts within the hit pixels is plotted against the array multiplicity. Both figures show a correlation between the brightness in the camera and the detector multiplicity of the array. It becomes apparent that only events A, B and C are bright within the array and the telescope (Figures 6.4, 6.5, 6.12). Considering the pictures in the camera these events have their center of gravity within the telescope and most properly the full shower and no subshower is recorded.

[10]The constant c in the used equation has to be calculated more precise.

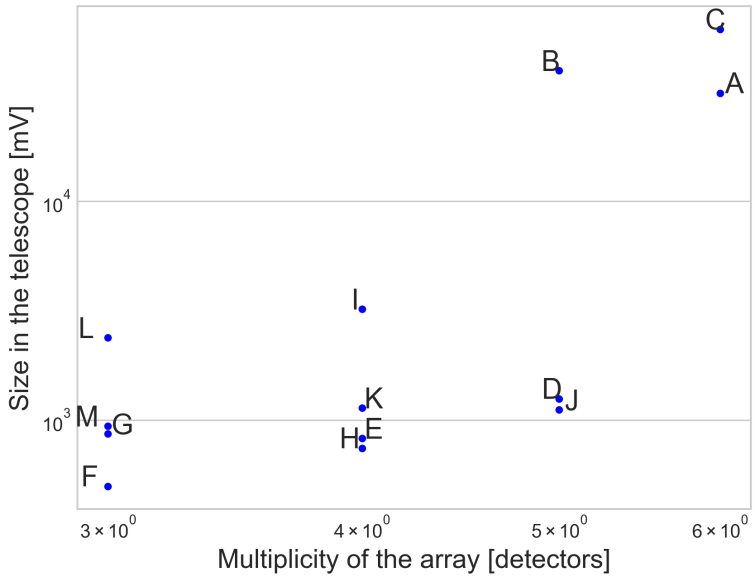

Figure 6.11: Correlation between the number of hit detectors in the array and the total signal height with in the area of the telescope for events measured and reconstructed in coincidence.

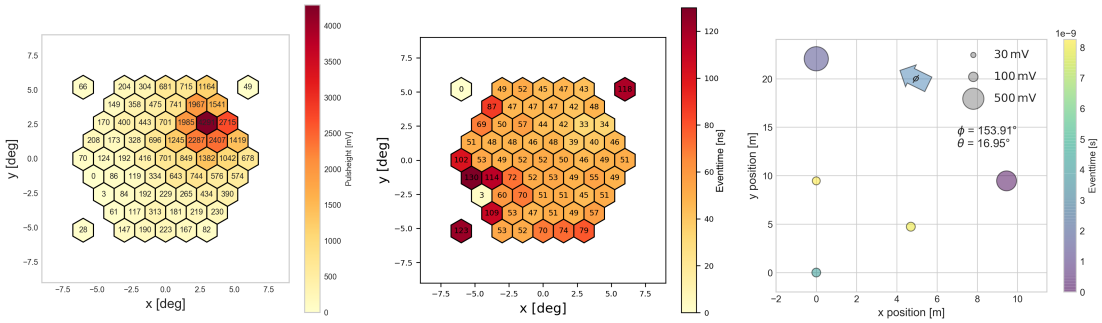

(a) Signal heights. **(b)** Timestamps. **(c)** Corresponding array event.

Figure 6.12: Event (B) in coincidence of the night of June 20^{th} 2018. $\phi_{FAMOUS} = 0.62°$, $\theta_{FAMOUS} = 2.67°$, A=54, l= 2.89°, w= 2.23°, $\delta = -2.842$.

For the further analysis especially events A, B and C are regarded, since these should be a precise measurement of the showers. These events are shown in Figures 6.4, 6.5 and 6.12 and highlighted in Figure 6.13.

Event A is already the only one with in the field of view from FAMOUS, event C is a little bit off but is in the field of view within the uncertainties. Event B is not close to the field of view from FAMOUS.

Since these events are within the camera and were detected with $w \approx l$, the distance between center of gravity (CoG) and the center of the camera is a better estimate for the zenith angle θ_{FAMOUS} than the disp method used up to this point. In Figure 6.14

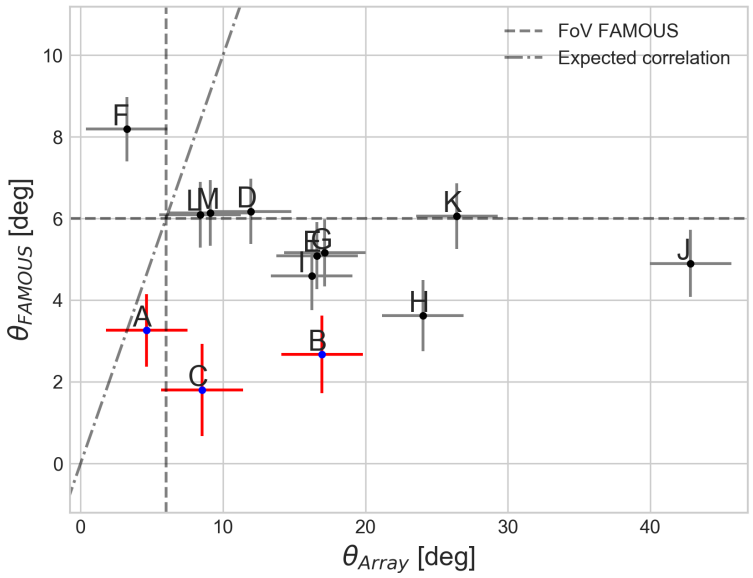

Figure 6.13: Correlation between the reconstructed zenith angle from FAMOUS and the air shower array. The dashdotted line symbolizes the expected correlation between the angles and the dashed lines mark the field of view from FAMOUS. The uncertainties are $\sigma_{FAMOUS} = 1.5°$ and $\sigma_{Array} = 2.9°$ as shown in [13] for vertical air showers. The highlighted datasets are considered for further analysis of the zenith angles.

the new zenith angles are shown. The uncertainty on θ_{FAMOUS} decreased since the calculation with $\theta_{FAMOUS} = \sqrt{x_{CoG}^2 + y_{CoG}^2}$ does not include variables or constants with high uncertainties.

As shown in Figure 6.14, the positions calculated with the CoG changed for each event in a different way. The distance between the expected correlation and event C' decreased and event A' further on in the field of view from FAMOUS. For event B' the measurements with the array have to be improved.

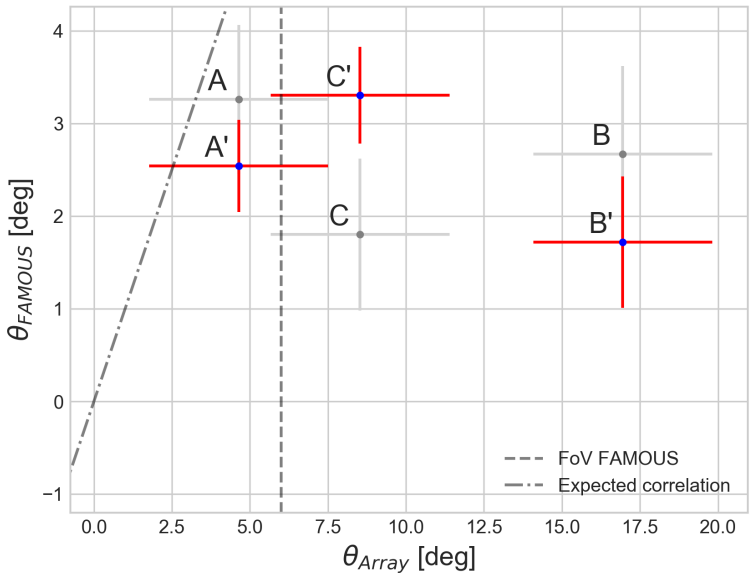

Figure 6.14: Correlation between the reconstructed zenith angle from FAMOUS and the air shower array. The dashdotted line symbolizes the expected correlation between the angles and the dashed lines mark the field of view from FAMOUS. The highlighted datasets are the newly calculated θ_{FAMOUS} with lower uncertainties than before, since the calculation for these round events is more precise.

7

Preparation for a laboratory course with a hybrid air shower detector

A coincidence measurement with the hybrid air shower detector will be implemented as a laboratory course during the master in physics at the RWTH. Possible setups and evaluations of the data where shown in chapters 5 and 6. In the following, other possible tasks and necessary adjustments on the roof and with the systems are explained.

7.1 Possible tasks for students

The measurements during the lab course will be a measurement in coincidence of the air shower array and the telescope FAMOUS on the roof.

In the lab course on particles and astroparticle physics, groups of two students have one experiment with measurements up to three days[1]. The goal of the lab course will not be to reconstruct the showers with the detectors individually. These are tasks for other experiments during the course [13, 20].

A challenge for preparation of the lab course will be to find a way to give the students the reconstruction of the showers hitting the air shower array without giving the detailed solution. A possibility could be to combine the experiments. The groups first have to participate in the experiment with the air shower array on the roof and have to measure with the hybrid detector afterwards as a second experiment. It has to be decided if the students are given a finished program which they can use for their analysis or they have

[1] At the time being.

to execute the methods themselves but the Hillas parametrization will be given in the introduction.

Another solution would be to have three groups: one having the air shower array, one group measures with the telescope and the last group combines the detectors and uses the solutions from the first groups to build up on. This would require the solutions of the first two groups to be correct or to give the correct solution to the third group. This method is difficult to incorporate into the existing concept of the lab courses since it requires lots of organizational measures. The timings of each experiment has to be set accordingly and the results have to be communicated between the different groups[2]. Additionally one group working with the air shower array or FAMOUS could not succeed with their analysis, giving the group with the hybrid detector a disadvantage during their analysis. Although this issue could be solved by giving the correct solutions to the last group.

For the small number of events it could be advisable to not hand the raw data to the group but rather give them the datasets which are created for the analysis of one event. The focus would lie on the connection between the events and not on the single reconstruction itself. Some of the necessary data sets would be the azimuthal and zenith angles, the event timestamps[3] and the highest sample for each hit detector or pixel. Lists having information on which detector was hit during which event for the air shower array would be very useful as well. With the information in these arrays plots similar to those in Figure 6.5 can be created and the events can be matched, since it is known when which detector was hit and which event took place at what time. For the telescope list with the leakage, the area and the size of each event would be advisable.

For the implementation of the lab course one should decide on the emphasis of the tasks. A possible focus could be the measurement itself and producing some correlation plots with the data. The students should think of a reasonable setup for the triggering of the hybrid detector. After discussing possible triggering systems with their supervisor they can execute the experimental assembly. In this case a challenge could be to synchronise the event times and matching the events in general as well as figuring out a setup.

Another focus of the task could be for the students to use the telescope in order to reconstruct events with only two hit detectors. The students would not only have to measure in coincidence but have to use the data to reconstruct additional events, too. It also would give another physical challenge to the students by using the knowledge about the reconstruction of both detectors and combining them. An add on would be that with this method more events in coincidence can be used and reconstructed, since most events will only hit two detectors in the array.

Alternatively, the focus could lay on the setup, where the students have to come up with an experimental assembly. The students could think about changing the setup in one way and discussing the consequences. One could vary the distance between the

[2]It would be useful for future jobs to have experience with this kind of group work, but it is not the goal in this lab course.

[3]In this case it would be possible to create a forced time shift so the students have a difficulty matching the events but both programs can run with the same computer.

air shower array and FAMOUS. According to [24], the detected events are larger for a greater distances at HAWC's Eye. This principle should be analogue for the local setup. The task could be to come up with an experiment, discuss the idea and expectations with the supervisor and analyse the outcome. This could happen in a smaller scenery as a bonus task for the students.

Retrospectively the reconstruction and analysis of the azimuthal angles is promising. It should be easy to specify the dataset and analysis. One could shift the angles and fit one line to all data points or calculate a more precise uncertainty on the angles. The correlation between the zenith angles should be specified in the future so the angles line up more precise.

7.2 Possible adjustments for the setup of the hybrid detector

For the lab course it would be useful to have a permanent setup on the roof for the telescope. This includes wires and cables to be led to the outsides by placing the wires through the exit in the roof or drilling another hole similar to the wiring placement of the air shower array. It includes a storage place for FAMOUS on the roof or in the room[4] leading to the roof. Depending on the main challenge of the lab course it would be useful to keep a flexible setup while doing this.

The triggering construction should be adjustable in order to try out several triggering systems. This would allow the students to switch the triggering system during one night of measurements as well. This is already given but for the lab course the different ports should be shown and explained in detail so the students can come up with a suitable setup.

To have an easier working environment with the hybrid detector, a detailed manual for the measurements with FAMOUS should be written. At the time being, starting a measurement with the telescope for a student who never worked with FAMOUS before is rather complicated. One could think about programming the start of a measurement more intuitive, since the focus of the lab course is not on the usage of FAMOUS but on the measurement with two detectors and the data analysis. Alternatively, a supervisor has to assist with starting that measurement.

Depending on the main task it would be nice to run the programs for the array and the telescope with the same computer. This would give the experimenters a nice overview on the incoming events and would help with the space coordination on the tables on the roof. This probably would solve the event matching issues since the timestamps will be according to the same clock and only will leave a small time difference due to the electrical delay. The delay can be overcome with other technical devices on two computers as well.

[4] Leading to the roof and to other rooms for facility management, there is a small room with the DAQ from the array and a computer with the programs for the array.

A challenge which has to be mastered is the weather dependency of the hybrid detector. In advance datasets of measurements in coincidence with different triggering setups should be recorded in order to give these to students who could not get useful data due to the weather. Also in preparation for the lab course measurements with bad weather conditions should be recorded and analysed in order to get an impression on the weather dependency.

It is advised to not give the raw data to the students but to hand the students lists with the necessary data as described before. A program which returns these lists or ROOT TTrees has to be written. It would be useful if the data will be saved directly in these files and the students do not have to run the raw data through the program.

As seen in Figure 6.9 the reconstruction of the zenith angles has to be improved. As shown e.g. events K and J have a high zenith angle from the array of $> 25°$. FAMOUS would not trigger for events in this area so the reconstruction from the array probably can be improved for the zenith angle. One should take a precise look into the reconstructions and check if there are more events with a reconstruction which does not seem plausible if one has more data points and statistics. In general it would be interesting to see more statistics for the azimuthal angle as well. It could be useful to reconstruct the array events with a center of gravity and another coordinate system analogue to the FAMOUS analysis in [20, 24].

8 Conclusion

During this thesis a future lab course with a hybrid air shower detector was discussed.

The hybrid detector is made up out of the imaging air-Cherenkov telescope FAMOUS and an air shower array on the roof of the Physikzentrum. FAMOUS detects Cherenkov light created by high energetic particles and air showers in the atmosphere while the array detects particles from air showers which pass the detector.

The thesis outlines the measurements with the array and the telescope singularly as well as an instruction on one method of reconstruction of the shower direction. Since the air shower array is a lab course too and another one is being constructed for the telescope, the analysis methods explained in this work are based on the sample solutions and instructions for each of the other courses [13, 20].

Measurements with two different setups were tested and analysed, both of which are usable in a lab course, whereas a setup where FAMOUS is triggered by the array is a simple solution since only a few events are saved and matching the events is rather easy. On the other hand, the second setup triggers both detectors individually and the triggering signal from FAMOUS is flagged. It would allow work with more datapoints and challenge the students to match the events as well as going through events which were not part of a coincidence.

During the analysis it became apparent that the two systems do not use a precise time stamp which forces the experimenter to match the events. This could be solved electronically rather easy by running both systems on the same computer which gives them the same time references. Apart from matching the events, it can be a challenge for the students to analyse the correlation plots, since the angle reconstructions from FAMOUS and the array are not evident. For the lab course, the students should be

advised to sort out the events, depending on which angle they are regarding, and only work with those which seem to have good qualities within the detectors, e.g. a high area and size for FAMOUS and a high multiplicity for the array.

This thesis can be used as an orientation while planning the lab course. It gives an general view on both detectors and explains the concepts. Possible setups are discussed and a potential task was solved by giving a short analysis of the results. Other achievable tasks are explained and discussed and some technical arrangements, which would help during the lab course, are listed.

Within the near future a new lab course can be created and the work with a SiPM based hybrid air shower detector would be an enrichment for interested students.

Acknowledgements - Danksagungen

During my work in this wonderful group I meet some impressing personalities who could help me a lot during times of troubles. I got lots of advice for my thesis and a load of work. I could not have done all the measurements with out you! Thank you all for making this work possible and helping when help is needed.

I enjoyed the times we had to work together and learn, program and understand the same things for different purposes. It would not have been the same without you.

Thanks to the wonderful people sharing an office with me, having heated discussions and almost missing appointments way to often. Great thanks to everybody who called for lunch and all nice and relaxing conversations while eating during a long day of work.

During times full of stress and work our small coffee breaks saved my day. It was the perfect time to reset and have small discourses about everything and anything.

On this note I want to end my acknowledgements to add all the people who helped me to get to this point in life. It was a great time with most of you and I am looking forward to continue this journey with you.

Bibliography

[1] Nobelprize.org. Nobel Prize in Physics 1936-Presentation Speech, Nobel Media AB 2014.

[2] W. Demtröder. *Experimentalphysik 4*. Experimentalphysik / Wolfgang Demtröder. Springer Berlin Heidelberg, 2006.

[3] H.V. Klapdor-Kleingrothaus and K. Zuber. *Particle Astrophysics*. Taylor & Francis, 1999.

[4] M. Tanabashi et al. (Particle Data Group). Review of Particle Physics (RPP). *Phys. Rev.*, D98:030001, 2018. 29. Cosmic Rays.

[5] NASA. National aeronautics and space administration. https://www.nasa.gov/content/fermi-gamma-ray-space-telescope, visited August 2018.

[6] Pierre Auger Collaboration. Pierre Auger Observatory. https://www.auger.org, visited August 2018.

[7] Marzena Lapka. CMS Knowledge Transfer: Cosmic rays. CMS Collection., Aug 2017.

[8] HAWC Collaboration. HAWC–The Hight-Altitude Water Cherenkov Gamma-Ray Observatory. https://www.hawc-observatory.org, August 2018.

[9] T. Bretz, T. Hebbeker, J. Kemp, L. Middendorf, T. Niggemann, C. Peters, M. Schaufel, J. Schumacher, J. Auffenberg, and C. Wiebusch. A compact and light-weight refractive telescope for the observation of extensive air showers. *ArXiv e-prints 1804.01781*, April 2018.

[10] Merlin Schaufel. HAWC's EYE-Implementing Hybrid detection by combining a compact air-Cherenkov Telescope with the HAWC Gamma-Ray Observatory. Master's thesis, RWTH Aachen University, III. Physikalisches Institut A, 2017.

[11] sense light. Introduction to SiPM, visited in August 2018. https://www.sensl.com/downloads/ds/TN%20-%20Intro%20to%20SPM%20Tech.pdf.

[12] C. D'Ambrosio. A short Overview on Scintillators. Lecture on Particle Detectors-Principles and Techniques, April 2015. CERN.

[13] Franziska Maria Tischbein. Measurement of cosmic air showers–a laboratory class experiment. Bachelors thesis, August 2018.

[14] Simon Weingarten. *Szintillationsdetektoren mit Silizium-Photomultipliern*. PhD thesis, RWTH Aachen University, III. Physikalisches Institut B, 2018.

[15] Donald L. (Placentia CA) Horrocks. Method and apparatus for determining random coincidence count rate in a scintillation counter utilizing the coincidence technique, January 1980. http://www.freepatentsonline.com/4181855.html.

[16] W. Demtröder. *Experimentalphysik 1*. Experimentalphysik / Wolfgang Demtröder. Springer, 2006.

[17] T. Niggemann, P. Assis, P. Brogueira, A. Bueno, H. M. Eichler, M. Ferreira, T. Hebbeker, M. Lauscher, L. Mendes, L. Middendorf, S. Navas, C. Peters, M. Pimenta, A. Ruiz, J. Schumacher, and M. Stephan. Status of the Silicon Photomultiplier Telescope FAMOUS for the Fluorescence Detection of UHECRs. *ArXiv e-prints 502.00792*, February 2015.

[18] Andreas Haungs. AugerNext: R&D; studies at the Pierre Auger Observatory for a next generation ground-based ultra-high energy cosmic ray experiment. *PoS*, ICRC2015:593, 2016.

[19] H Anderhub, M Backes, A Biland, A Boller, I Braun, T Bretz, V Commichau, L Djambazov, D Dorner, C Farnier, A Gendotti, O Grimm, H P von Gunten, D Hildebrand, U Horisberger, B Huber, K S Kim, J H Köhne, T Krähenbühl, B Krumm, M Lee, J P Lenain, E Lorenz, W Lustermann, E Lyard, K Mannheim, M Meharga, D Neise, F Nessi-Tedaldi, A K Overkemping, F Pauss, D Renker, W Rhode, M Ribordy, R Rohlfs, U Röser, J P Stucki, J Thaele, O Tibolla, G Viertel, P Vogler, R Walter, K Warda, and Q Weitzel. Electronics for the camera of the First G-APD Cherenkov Telescope (FACT) for ground based gamma-ray astronomy. *Journal of Instrumentation*, 7(01):C01073, 2012.

[20] Terry Generet. HAWC's Eye as a Lab Course Telescope–Proof of Concept. Bachelors thesis, July 2018.

[21] A. M. Hillas. Cerenkov light images of EAS produced by primary gamma. *International Cosmic Ray Conference*, 3, 1985.

[22] Sven Günther. Private conversations, July 2018.

[23] Steffen Thorsen. Time and Date AS. https://www.timeanddate.com/sun/germany/aachen, visited Aug. 2018.

[24] Sven Günther. First hybrid reconstruction of the arrival direction with HAWC's Eye. Bachelors Thesis, August 2018.

Eidesstattliche Versicherung
Statutory Declaration in Lieu of an Oath

_____ _____

Name, Vorname/Last Name, First Name

Matrikelnummer (freiwillige Angabe)
Matriculation No. (optional)

Ich versichere hiermit an Eides Statt, dass ich die vorliegende Arbeit/Bachelorarbeit/ Masterarbeit* mit dem Titel
I hereby declare in lieu of an oath that I have completed the present paper/Bachelor thesis/Master thesis* entitled

_____

_____

_____

selbstständig und ohne unzulässige fremde Hilfe (insbes. akademisches Ghostwriting) erbracht habe. Ich habe keine anderen als die angegebenen Quellen und Hilfsmittel benutzt. Für den Fall, dass die Arbeit zusätzlich auf einem Datenträger eingereicht wird, erkläre ich, dass die schriftliche und die elektronische Form vollständig übereinstimmen. Die Arbeit hat in gleicher oder ähnlicher Form noch keiner Prüfungsbehörde vorgelegen.
independently and without illegitimate assistance from third parties (such as academic ghostwriters). I have used no other than the specified sources and aids. In case that the thesis is additionally submitted in an electronic format, I declare that the written and electronic versions are fully identical. The thesis has not been submitted to any examination body in this, or similar, form.

_____ _____

Ort, Datum/City, Date

Unterschrift/Signature

*Nichtzutreffendes bitte streichen

*Please delete as appropriate

Belehrung:
Official Notification:

§ 156 StGB: Falsche Versicherung an Eides Statt
Wer vor einer zur Abnahme einer Versicherung an Eides Statt zuständigen Behörde eine solche Versicherung falsch abgibt oder unter Berufung auf eine solche Versicherung falsch aussagt, wird mit Freiheitsstrafe bis zu drei Jahren oder mit Geldstrafe bestraft.
Para. 156 StGB (German Criminal Code): False Statutory Declarations
Whoever before a public authority competent to administer statutory declarations falsely makes such a declaration or falsely testifies while referring to such a declaration shall be liable to imprisonment not exceeding three years or a fine.
§ 161 StGB: Fahrlässiger Falscheid; fahrlässige falsche Versicherung an Eides Statt
(1) Wenn eine der in den §§ 154 bis 156 bezeichneten Handlungen aus Fahrlässigkeit begangen worden ist, so tritt Freiheitsstrafe bis zu einem Jahr oder Geldstrafe ein.
(2) Straflosigkeit tritt ein, wenn der Täter die falsche Angabe rechtzeitig berichtigt. Die Vorschriften des § 158 Abs. 2 und 3 gelten entsprechend.
Para. 161 StGB (German Criminal Code): False Statutory Declarations Due to Negligence
(1) If a person commits one of the offences listed in sections 154 through 156 negligently the penalty shall be imprisonment not exceeding one year or a fine.
(2) The offender shall be exempt from liability if he or she corrects their false testimony in time. The provisions of section 158 (2) and (3) shall apply accordingly.

Die vorstehende Belehrung habe ich zur Kenntnis genommen:
I have read and understood the above official notification:

_____ _____

Ort, Datum/City, Date

Unterschrift/Signature

A Appendix

Regarding: Air shower array

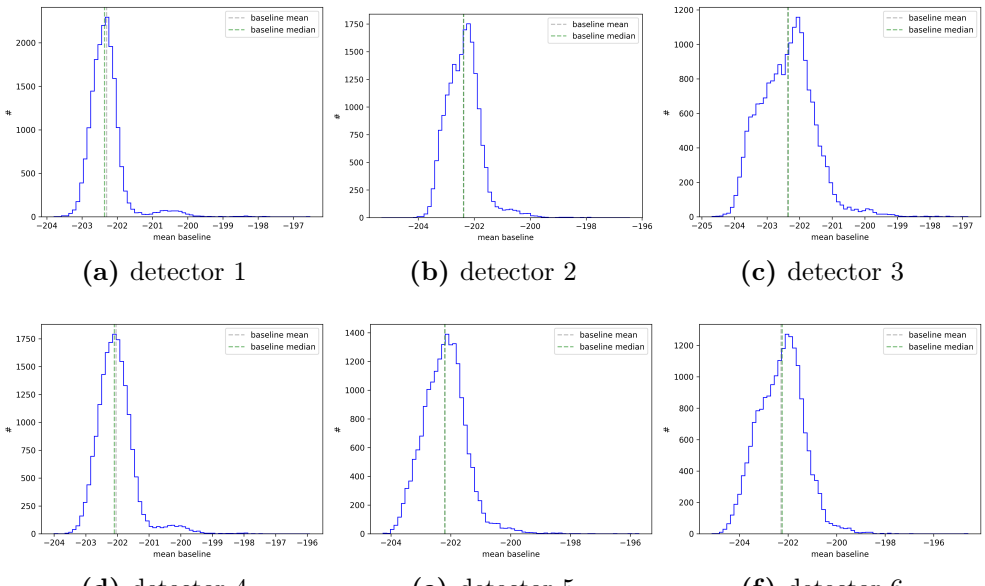

(a) detector 1 **(b)** detector 2 **(c)** detector 3

(d) detector 4 **(e)** detector 5 **(f)** detector 6

Figure A.1: Regarding chapter 3: Uncorrected baseline for each detector. For these histograms for each event the mean of first 200 voltage samples are calculated.

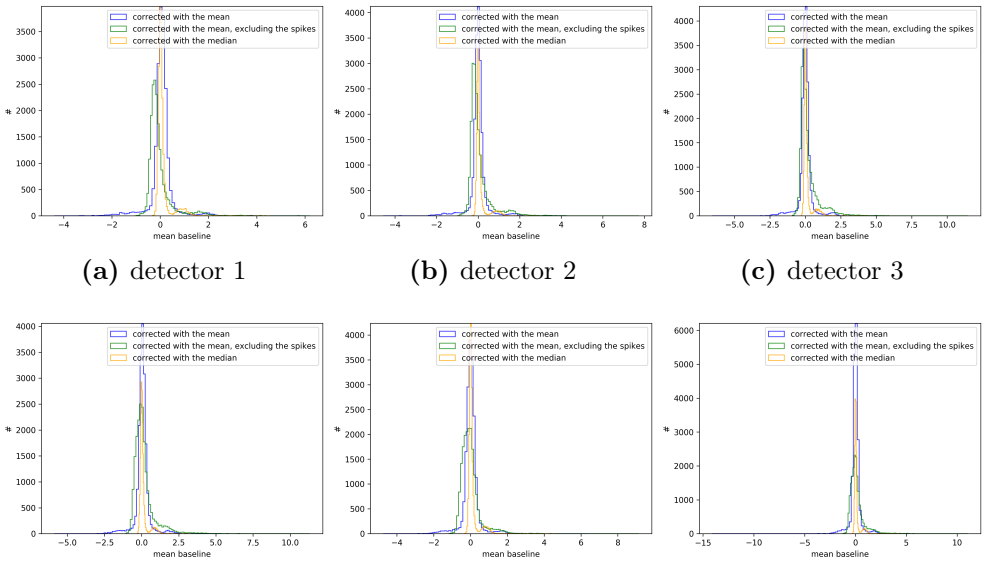

(a) detector 1 **(b)** detector 2 **(c)** detector 3

(d) detector 4 **(e)** detector 5 **(f)** detector 6

Figure A.2: Regarding chapter 3:Histogram of the baseline mean for each detector. The asymmetric increase on the right side is due to irregular spikes in the voltage data as seen in fig. 3.4. These spikes appear due to the boards and are by passed with the median in the correction.

Regarding: Measuring in coincidence with FAMOUS and the air shower array

Measurement from June 20^{th}

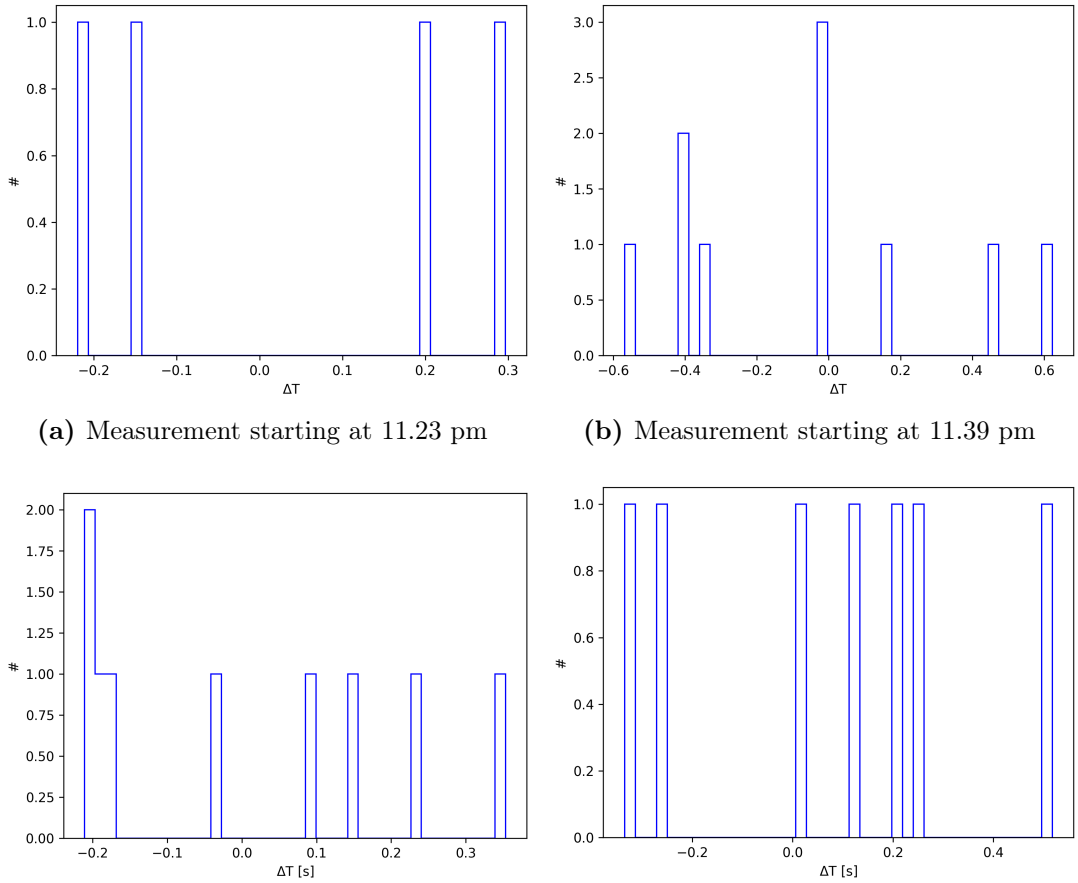

(a) Measurement starting at 11.23 pm

(b) Measurement starting at 11.39 pm

(c) Measurement starting at 00.26 am

(d) Measurement starting at 00.57 am

Figure A.3: Time differences between the array and the FAMOUS time stamps after correcting the time shift for events measured in coincidence.

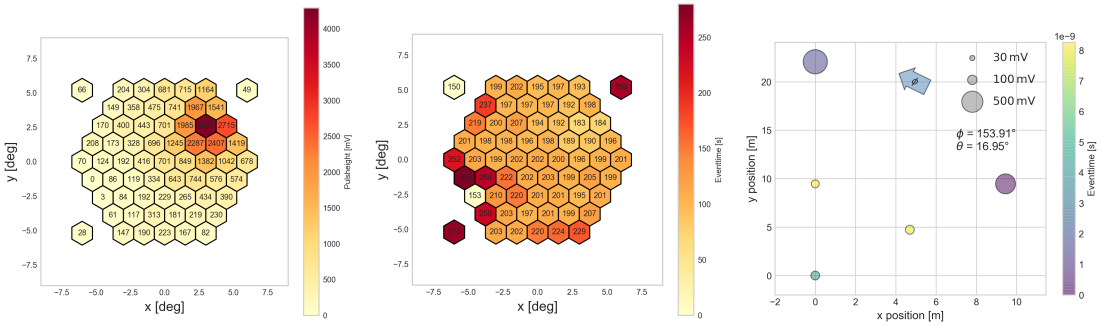

(a) signal heights

(b) timestamps

(c) Corresponding array event

Figure A.4: Event (B) in coincidence of the night of June 20^{th} 2018. $\phi_{FAMOUS} = 37.99°$, $\theta_{FAMOUS} = 2.67°$, A=54, l= 2.89°, w= 2.23°, $\delta = -2.842$.

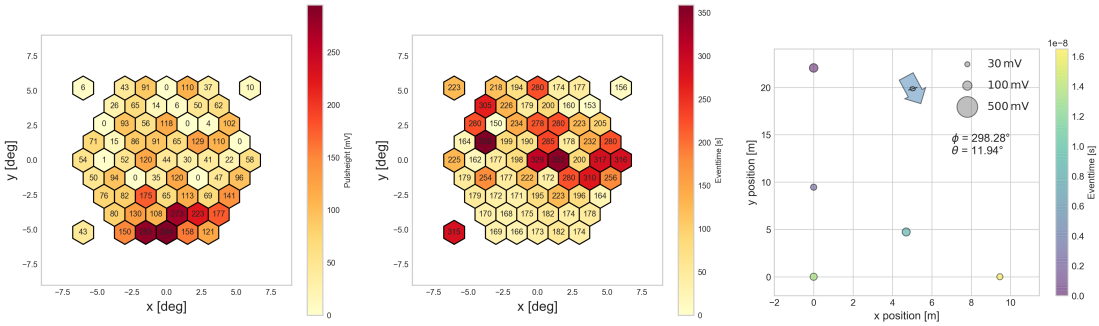

(a) signal heights **(b)** timestamps **(c)** Corresponding array event

Figure A.5: Event (D) in coincidence of the night of June 20^{th} 2018. $\phi_{FAMOUS} = -115.39°$, $\theta_{FAMOUS} = 6.17°$, A=5, l= 1.16°, w= 0.73°, $\delta = 0.062$.

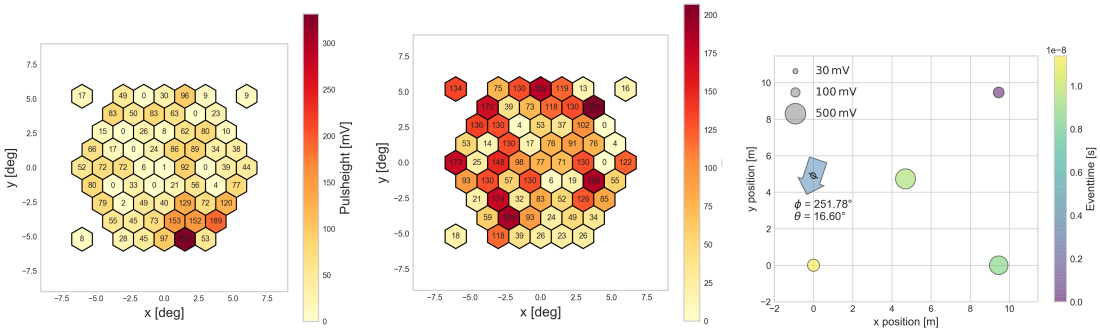

(a) signal heights **(b)** timestamps **(c)** Corresponding array event

Figure A.6: Event (E) in coincidence of the night of June 20^{th} 2018. $\phi_{FAMOUS} = -89.5°$, $\theta_{FAMOUS} = 5.09°$, A=4, l= 1.16°, w= 0.67°, $\delta = 0.328$.

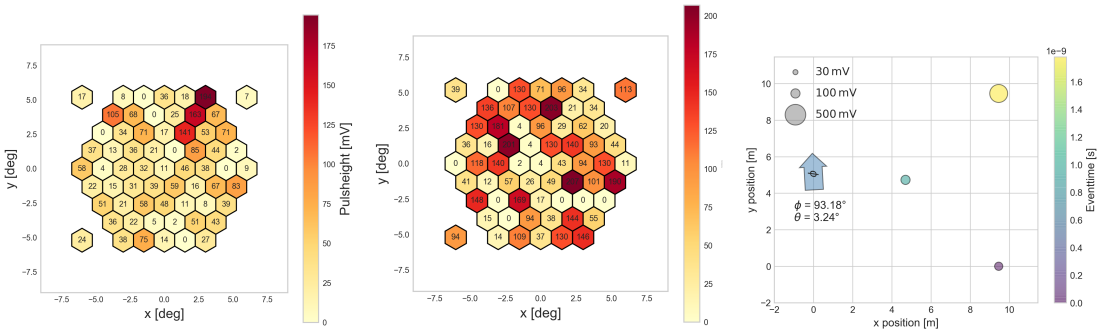

(a) signal heights **(b)** timestamps **(c)** Corresponding array event

Figure A.7: Event (F) in coincidence of the night of June 20^{th} 2018. $\phi_{FAMOUS} = 60.0°$, $\theta_{FAMOUS} = 8.19°$, A=3, l= 1.28°, w= 0.38°, $\delta = -2.094$.

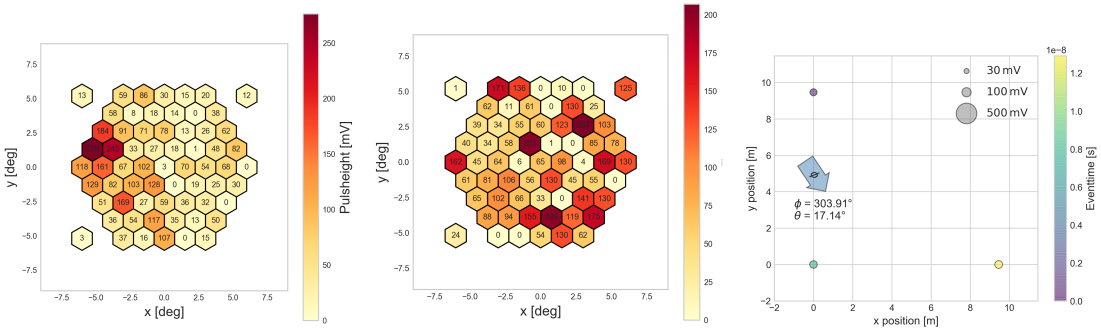

(a) signal heights **(b)** timestamps **(c)** Corresponding array event

Figure A.8: Event (G) in coincidence of the night of June 20^{th} 2018. $\phi_{FAMOUS} = 151.11°$, $\theta_{FAMOUS} = 5.16°$, A=4, l= 0.90°, w= 0.69°, $\delta = -1.574$.

Measurement from June 26^{th}

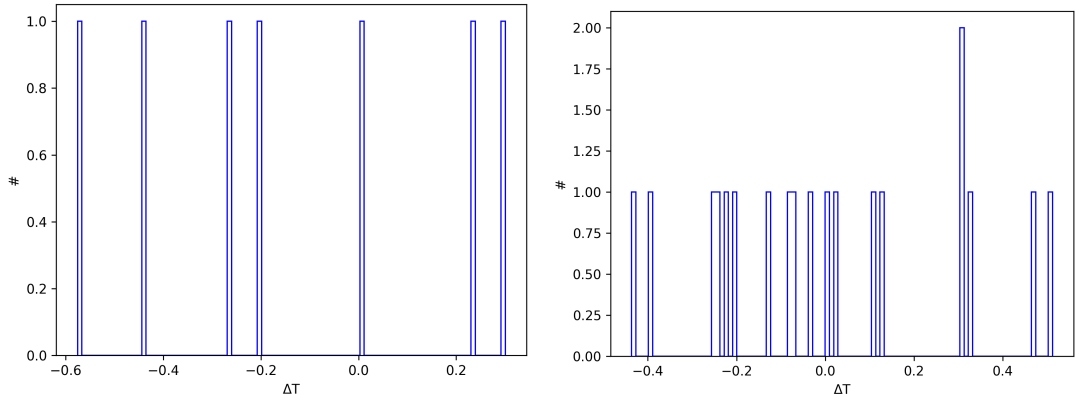

(a) Measurement starting at 00.59 am **(b)** Measurement starting at 1.40 am

Figure A.9: Time differences between the array and the FAMOUS time stamps after correcting the time shift for events measured in coincidence.

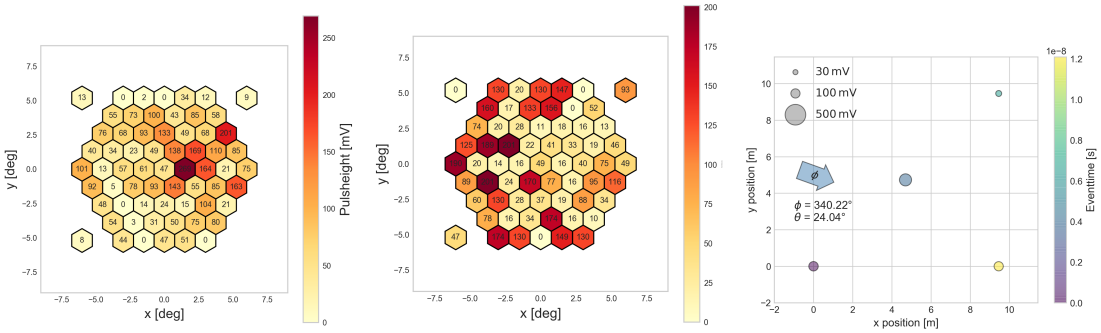

(a) signal heights **(b)** timestamps **(c)** Corresponding array event

Figure A.10: Event (H) in coincidence of the night of June 26^{th} 2018. $\phi_{FAMOUS} = 26.57°$, $\theta_{FAMOUS} = 3.62°$, A=4, l= 1.09°, w= 0.63°, $\delta = -2.292$.

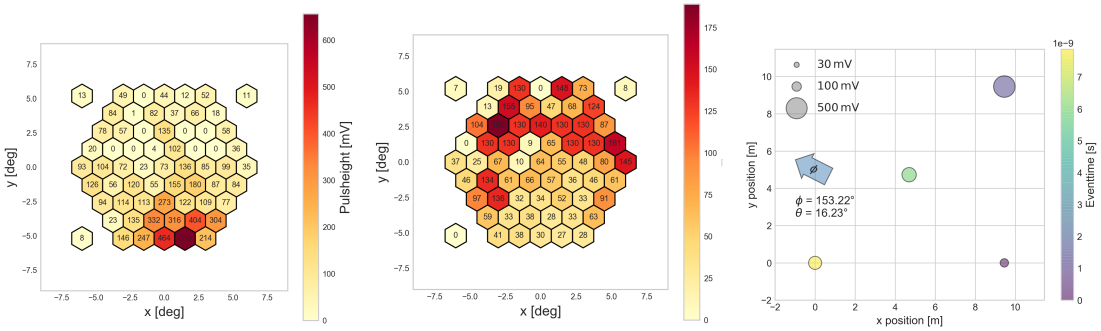

(a) signal heights **(b)** timestamps **(c)** Corresponding array event

Figure A.11: Event (I) in coincidence of the night of June 26^{th} 2018. $\phi_{FAMOUS} = -102.95°$, $\theta_{FAMOUS} = 4.59°$, A=9, l= 1.55°, w= 0.91°, $\delta = 0.022$.

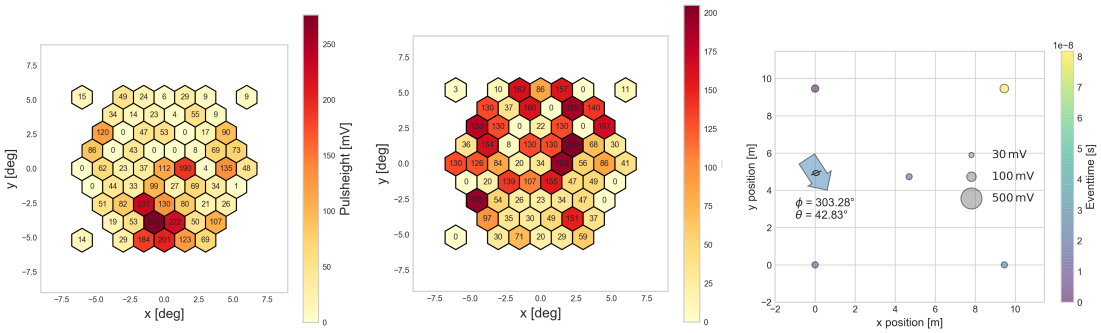

(a) signal heights **(b)** timestamps **(c)** Corresponding array event

Figure A.12: Event (J) in coincidence of the night of June 26^{th} 2018. $\phi_{FAMOUS} = -90.65°$, $\theta_{FAMOUS} = 4.90°$, A=5, l= 1.08°, w= 0.87°, $\delta = 2.150$.

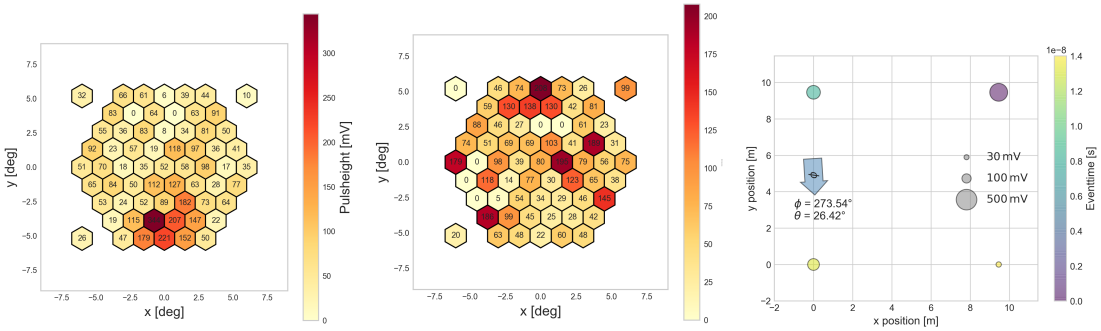

(a) signal heights **(b)** timestamps **(c)** Corresponding array event

Figure A.13: Event (K) in coincidence of the night of June 26^{th} 2018. $\phi_{FAMOUS} = -108.65°$, $\theta_{FAMOUS} = 6.06°$, A=5, l= 1.28°, w= 0.65°, $\delta = 0.711$.

Measurement from July 13^{th}

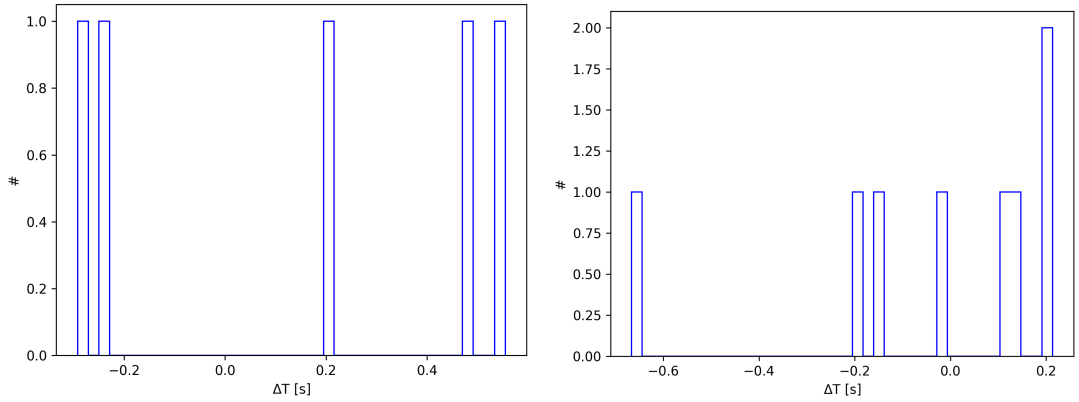

(a) Measurement starting at 2.39 am **(b)** Measurement starting at 3.03 am

Figure A.14: Time differences between the array and the FAMOUS time stamps after correcting the time shift for events measured in coincidence.

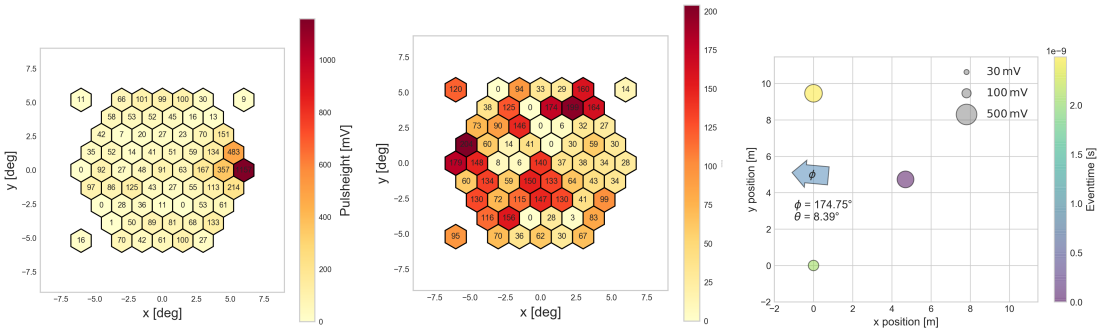

(a) Signal heights. **(b)** Timestamps. **(c)** Corresponding array event.

Figure A.15: Event (L) in coincidence of the night of July 13^{th} 2018. $\theta_{FAMOUS} = 6.09°$, $\phi_{FAMOUS} = 0.97°$ A=5 pixels, l= 0.921°, w= 0.783°, $\delta = 3.0832$.

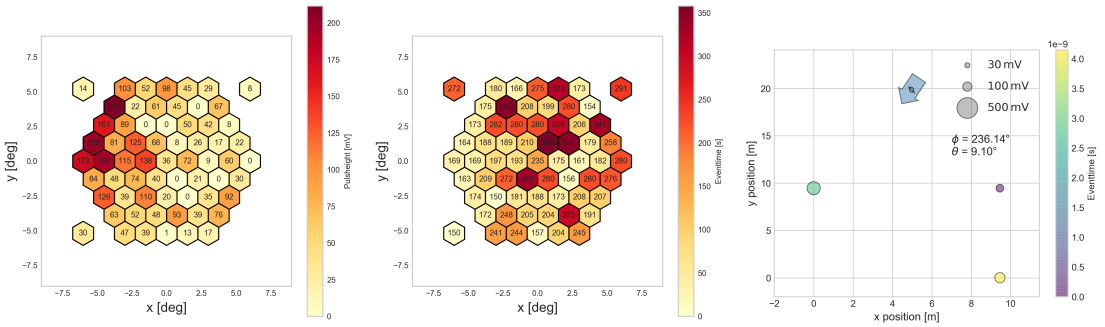

(a) signal heights **(b)** timestamps **(c)** Corresponding array event

Figure A.16: Event (M) in coincidence of the night of July 13^{th} 2018. $\phi_{FAMOUS} = -167.14°$, $\theta_{FAMOUS} = 6.14°$, A=5, l= 1.13°, w= 0.73°, $\delta = 3.068$.